Research Square

Preprints are preliminary reports that have not undergone peer review.
They should not be considered conclusive, used to inform clinical practice,
or referenced by the media as validated information.

Panel-Gene Transcriptomic Associations in Multiple Sclerosis: a three-cohort white-matter analysis of a locked 468-gene detoxification panel

Mark E. McCaulley

mark@siriusneuroscience.com

Sirius Neuroscience, LLC https://orcid.org/0000-0003-2059-622X

Research Article

Keywords: multiple sclerosis, white matter, transcriptomics, meta-analysis, heme oxygenase-1, iron, glutathione, oxidative stress

Posted Date: October 29th, 2026

DOI: https://doi.org/10.21203/rs.3.rs-11530178/v1

License: This work is licensed under a Creative Commons Attribution 4.0 International License.
Read Full License

Additional Declarations: The authors declare potential competing interests as follows: The author is the sole inventor on a filed patent application relating to panel-based research scoring methods that use the locked 468-gene list reported here. The application did not determine gene membership, the high-confidence rule, or the reported results. Academic reuse of the deposited panel and code does not require a license from the author. The author declares no other competing interests.

Abstract

Multiple sclerosis (MS) was examined with a locked 468-gene redox, metal, xenobiotic-metabolism and barrier panel in three adult white-matter cohorts from the Gene Expression Omnibus (GSE138614, GSE32915, GSE108000). A DerSimonian–Laird random-effects meta-analysis yielded 442 analyzable genes, 78 at Benjamini–Hochberg FDR < 0.05, and 30 high-confidence genes (FDR < 0.05, measured in ≥ 3 cohorts, direction-concordant in ≥ 70% of contributing cohorts, and nominally significant in ≥ 2 cohorts); 12 were higher in MS, led by CP and PPARG, and 18 lower, led by OPLAH and GAMT. The meta-analysis was reproduced exactly from the per-cohort GEO2R result tables. Panel genes were not more often FDR-significant than the rest of the transcriptome (17.2% versus 15.5%; Fisher P = 0.35), and 18% of 20,000 random sets of 442 measured genes had at least as many FDR-significant genes as the panel. Each cohort contributes several samples per donor; re-fitted with the donor as the unit, 17 genes met the high-confidence rule, 12 of them from the original 30, and adjustment for an oligodendrocyte marker score left 9. Under a Hartung–Knapp–Sidik–Jonkman test no gene reached FDR < 0.05. In an independent cohort (GSE123496), 25 of the 30 high-confidence genes changed in the same direction (exact binomial p = 0.0003; Pearson r = 0.73). In supporting lesion and grey-matter tiers (not pooled), higher HMOX1 and lower GPX4 (the latter not FDR-significant in the meta-analysis) recurred; oligodendrocyte loss with glial and vascular expansion may explain part of these and other signals. These are transcript-abundance associations in postmortem tissue; enzyme activity, iron content and lipid peroxidation were not measured, and the findings do not establish ferroptosis or a treatment target.

What this analysis reports

In MS white matter the panel does not move as a block; it splits in two directions. Iron-handling and stress-response transcripts are higher — ceruloplasmin (CP) +1.36, PPARG +0.96, ferritin light chain (FTL) +0.89, HMOX1 +0.88 and AKR1C3 +0.76 log2 units — while the transferrin receptor (TFRC) is lower (−0.39); ceruloplasmin supports iron export and ferritin iron storage, so these transcripts alone do not show whether tissue iron is being retained or released. Transcripts of routine conjugation, glutathione handling and one-carbon metabolism are lower, led by OPLAH (−1.24) and GAMT (−1.06) and followed by G6PD (−0.70), ALDH1A3 (−0.60), GSTZ1 (−0.51) and CYP26A1 (−0.41). Twelve of the 30 high-confidence genes are higher and 18 lower, and 25 of the 30 move the same way in an independent cohort. Lesions lose oligodendrocytes and gain microglia, astrocytes and vascular cells, so part of this pattern may reflect tissue composition rather than change within cells, and because each cohort contributes several samples per donor, per-gene P values are optimistic. Panel genes change little more often than the rest of the transcriptome. Re-fitted with the donor as the unit, 12 of the 30 remain high-confidence (among them OPLAH, GAMT, PPARG, CP and CYP2A7), and adjustment for oligodendrocyte content leaves few. Fifteen panel genes already differ in normal-appearing white matter, where no demyelination is visible histologically; this is the least secure result, because its 21 NAWM and 25 control samples come from 7 MS donors and 5 control donors, and none of the 15 remains significant when re-fitted with the donor as the unit. Every number here is transcript abundance in postmortem bulk tissue; enzyme activity, iron content and lipid peroxidation were not measured.

Introduction

Multiple sclerosis is a chronic inflammatory and neurodegenerative disease of the central nervous system that affects an estimated 2.8 million people worldwide (2). Its course passes through relapsing-remitting, secondary progressive and primary progressive phases; immunomodulatory therapies are most effective in the relapsing phase and have limited efficacy against progressive neurodegeneration (3–5). Its pathological hallmarks include focal white-matter demyelinating plaques, diffuse abnormalities of normal-appearing white matter (NAWM), and cortical grey-matter lesions that correlate with cognitive impairment and progressive disability (4).

The companion analyses of this series apply one locked 468-gene panel representing the cell's xenobiotic-detoxification, antioxidant-defence, metal-homeostasis and blood-brain-barrier machinery. The panel was assembled by complete functional-family enumeration, not by data-driven selection: all human cytochrome P450s, glutathione S-transferases, UDP-glucuronosyltransferases, sulfotransferases and related conjugation enzymes; the glutathione, thioredoxin, peroxiredoxin, superoxide-dismutase, catalase and glutathione-peroxidase systems and the KEAP1–NFE2L2 (NRF2) axis; metallothioneins and metal- and iron-homeostasis genes; and the blood-brain-barrier tight-junction, adhesion and transporter module. It builds on the detoxification signature of the foundation study (6). The panel was not derived from the XenoReg detoxification and physiological-barrier gene set of Santos et al. (7); overlap with that 519-gene set was inspected after the freeze and was not used to add or remove genes. Membership was set by functional-family rules and pre-specified filters; the genes added at the panel freeze, and the MS result without them, are given in Methods. The panel definition and the cross-disease synthesis are reported in the methods-and-panel manuscript (1) and deposited at Zenodo (8).

MS is informative for this panel for four reasons. First, dimethyl fumarate, an NRF2-pathway drug, is approved for relapsing MS, with roughly halved annualized relapse rates in phase 3 trials (9, 10); that approval is background pharmacology, not validation of this panel. Second, MS lesions pass through histologically defined stages that can be compared with control tissue in one series. Third, the published HMOX1 literature is context-dependent by lesion stage; these data measure transcript abundance, not whether that response is protective or harmful. Fourth, ferroptosis has been reported in MS and its models (11–15), neuronal STING signalling has been linked to MS neurodegeneration and ferroptosis pathways (17, 18), and STING has been shown to target GPX4 for degradation in myocardial ischaemia–reperfusion injury (16); these transcript data measure neither ferroptosis nor STING activity.

The objective is to report the locked three-cohort white-matter meta-analysis, to check its high-confidence set in an independent cohort, and to place supporting lesion-stage, lesion-zone, grey-matter and composition analyses in context. This is not claimed as a complete characterization of the pathway family in MS.

Results

Study design and panel coverage

Primary inference is a random-effects meta-analysis of three MS-versus-control white-matter cohorts: GSE138614 (RNA-seq; 73 samples of normal-appearing white matter and four lesion types from 10 patients with progressive MS, and 25 control white-matter samples from 5 donors) (19), GSE32915 (Agilent microarray; 12 samples of normal-appearing white matter and lesion areas from four patients with acute MS, and white matter from four controls) (20) and GSE108000 (Agilent microarray; rim and perilesional samples from 7 chronic active and 8 inactive lesions, and white matter from 10 control donors) (21). Each cohort therefore contributes more than one sample per MS donor or lesion (see Limitations). Measurable panel-gene coverage was 386 of 468 in GSE138614, 435 in GSE32915 and 436 in GSE108000. Supporting tiers, none of which enters the pooled estimate, are the GSE138614 lesion-type contrasts, the four GSE108000 lesion-zone contrasts, the cortical grey-matter series GSE135511 (follicle-stratified; 370–373 measurable panel genes per contrast) (22) and GSE131279 (a within-MS lesion-versus-normal-appearing grey-matter contrast and one of the two sub-series of GSE131282; 448 measurable) (23), and cell-type composition from the single-nucleus atlas of Macnair et al. (632,375 nuclei, of which 335,694 are white matter and carry the lesion-type assignments used here) (24). An independent multi-region brain RNA-seq cohort, GSE123496 (25), was used only to check the high-confidence set. Four candidate datasets were excluded: GSE5839 (a single control array), GSE38010 (non-log-transformed values), GSE52139 (a within-MS spinal-cord contrast without non-MS controls) and the grey-matter SuperSeries GSE131282 (a transcriptome-wide scale offset; see below). Its control-containing sub-series, GSE131281 (normal-appearing versus control grey matter; 452 measurable), is reported alone as a supporting contrast, and the optic-chiasm series GSE100297 was analyzed but not used further (Methods). The screen that identified these cohorts is documented in Table S1.

Primary three-cohort white-matter meta-analysis

Of the 468 panel genes, 442 were meta-analyzable (measured in at least two of the three cohorts), 78 reached Benjamini–Hochberg FDR < 0.05, and 30 met the locked high-confidence rule: FDR < 0.05, measured in ≥ 3 cohorts, direction-concordant in ≥ 70% of contributing cohorts, and nominally significant in ≥ 2 cohorts (Table 1, Fig. 1). Twelve high-confidence genes were higher and 18 lower in MS white matter. Median I^2 among the 30 was 0%, and 20 of the 30 had I^2 of 0%; with three cohorts, I^2 is estimated imprecisely, so these values do not by themselves establish agreement between cohorts. The full set of 78 FDR-significant genes is given in Table S2 and all 442 genes in Data S1.

Table 1

High-confidence panel genes in the three-cohort white-matter meta-analysis (k = 3). Pooled log2 fold-change (MS vs control white matter) by DerSimonian–Laird random effects across GSE138614, GSE32915 and GSE108000; 95% CI = pooled estimate ± 1.96 × SE; I^2 = between-cohort heterogeneity; P = two-sided; FDR = Benjamini–Hochberg across 442 meta-analyzable genes. All 30 genes were measured in all three cohorts. High-confidence rule: FDR < 0.05, measured in ≥ 3 cohorts, direction-concordant in ≥ 70% of contributing cohorts, nominally significant in ≥ 2 cohorts. Values are full precision from the reproduction of the locked analysis (Data S1); pooled estimates, I^2 and FDR status agree with the locked file for all 442 genes. Twenty-six of the 30 are CORE-tier genes (including FXN and TFRC from the ferroptosis/iron/NRF2 group and TREX1 from the cGAS–STING group) and 4 belong to the SENSITIVITY layer (CYCS, TUFM, UBB, XBP1). The 78 FDR-significant genes are in Table S2.

Gene	Direction	Pooled log2FC	95% CI	I^2 (%)	P	FDR	Function
CP	Higher	+ 1.36	+ 0.41 to + 2.32	89.0	0.005	0.032	Ceruloplasmin; ferroxidase, iron export
PPARG	Higher	+ 0.96	+ 0.75 to + 1.17	0.0	2.1×10^{-19}	3.1×10^{-17}	Nuclear receptor; lipid and inflammatory signalling
FTL	Higher	+ 0.89	+ 0.59 to + 1.20	0.0	1.2×10^{-8}	5.2×10^{-7}	Ferritin light chain; iron storage
HMOX1	Higher	+ 0.88	+ 0.53 to + 1.23	0.0	1.1×10^{-6}	2.7×10^{-5}	Heme oxygenase 1; heme degradation, NRF2 target
AKR1C3	Higher	+ 0.76	+ 0.49 to + 1.03	0.0	4.3×10^{-8}	1.6×10^{-6}	Aldo-keto reductase; NRF2 target
ALDH1L2	Higher	+ 0.73	+ 0.33 to + 1.12	69.4	2.9×10^{-4}	0.003	Mitochondrial 10-formyl-THF dehydrogenase; one-carbon
XBP1	Higher	+ 0.72	+ 0.38 to + 1.06	32.2	2.8×10^{-5}	4.2×10^{-4}	ER-stress transcription factor
PECAM1	Higher	+ 0.69	+ 0.21 to + 1.17	73.2	0.0046	0.03	Endothelial adhesion (barrier module)
GPX1	Higher	+ 0.66	+ 0.31 to + 1.00	0.0	1.9×10^{-4}	0.0021	Glutathione peroxidase 1
MGST2	Higher	+ 0.58	+ 0.37 to + 0.78	0.0	3.8×10^{-8}	1.5×10^{-6}	Microsomal glutathione S-transferase 2
SLC7A11	Higher	+ 0.51	+ 0.19 to + 0.82	9.7	0.0015	0.012	Cystine/glutamate antiporter (xCT)

Gene	Direction	Pooled log2FC	95% CI	I^2 (%)	P	FDR	Function
NAT1	Higher	+ 0.39	+ 0.21 to + 0.57	0.0	2.5×10^{-5}	3.9×10^{-4}	N-acetyltransferase 1; conjugation
FXN	Lower	-0.22	-0.32 to -0.13	0.0	5.0×10^{-6}	1.0×10^{-4}	Frataxin; iron–sulfur cluster assembly
UBB	Lower	-0.30	-0.47 to -0.13	0.0	4.8×10^{-4}	0.0049	Ubiquitin B
SLC39A3	Lower	-0.34	-0.46 to -0.21	0.0	2.0×10^{-7}	5.9×10^{-6}	Zinc importer ZIP3
CBS	Lower	-0.35	-0.56 to -0.14	29.5	9.7×10^{-4}	0.0082	Cystathionine β-synthase; transsulfuration
TFRC	Lower	-0.39	-0.62 to -0.16	0.0	9.2×10^{-4}	0.0082	Transferrin receptor; iron import
ALDH1L1	Lower	-0.39	-0.62 to -0.16	0.0	8.6×10^{-4}	0.0078	10-formyl-THF dehydrogenase; one-carbon
CYP26A1	Lower	-0.41	-0.65 to -0.17	0.0	6.4×10^{-4}	0.0063	Retinoic acid hydroxylase
TUFM	Lower	-0.45	-0.58 to -0.32	3.7	5.1×10^{-12}	4.5×10^{-10}	Mitochondrial elongation factor Tu
TREX1	Lower	-0.46	-0.66 to -0.26	0.0	6.0×10^{-6}	1.1×10^{-4}	3'-exonuclease; cGAS–STING arm
CGN	Lower	-0.48	-0.72 to -0.25	0.0	6.2×10^{-5}	8.2×10^{-4}	Cingulin; tight junction
ATOX1	Lower	-0.48	-0.63 to -0.33	0.0	1.7×10^{-10}	9.2×10^{-9}	Copper chaperone
GSTZ1	Lower	-0.51	-0.72 to -0.30	0.0	2.6×10^{-6}	5.8×10^{-5}	Glutathione S-transferase zeta 1
CYCS	Lower	-0.52	-0.74 to -0.30	13.1	2.6×10^{-6}	5.8×10^{-5}	Cytochrome c; respiratory chain

Gene	Direction	Pooled log2FC	95% CI	I^2 (%)	P	FDR	Function
ALDH1A3	Lower	-0.60	-0.78 to -0.42	0.0	2.4×10^{-11}	1.7×10^{-9}	Retinaldehyde dehydrogenase 3
CYP2A7	Lower	-0.61	-0.98 to -0.24	63.2	0.0012	0.0093	Cytochrome P450 2A7
G6PD	Lower	-0.70	-0.88 to -0.51	13.2	1.8×10^{-13}	1.9×10^{-11}	Pentose-phosphate pathway; NADPH
GAMT	Lower	-1.06	-1.28 to -0.83	0.0	1.7×10^{-20}	3.7×10^{-18}	Guanidinoacetate methyltransferase; creatine synthesis
OPLAH	Lower	-1.24	-1.49 to -1.00	0.0	6.1×10^{-23}	2.7×10^{-20}	5-oxoprolinase; glutathione cycle

The higher arm is dominated by iron handling and stress-responsive transcripts: CP (+ 1.36), PPARG (+ 0.96), FTL (+ 0.89), HMOX1 (+ 0.88), AKR1C3 (+ 0.76), ALDH1L2 (+ 0.73), XBP1 (+ 0.72), PECAM1 (+ 0.69), GPX1 (+ 0.66), MGST2 (+ 0.58), the cystine/glutamate antiporter SLC7A11 (+ 0.51) and NAT1 (+ 0.39). Several further iron- and NRF2-related transcripts were FDR-significant without meeting the high-confidence rule, including ferroportin SLC40A1 (+ 0.56), NQO1 (+ 0.49, measured in two cohorts) and ICAM1 (+ 0.67). The lower arm comprises glutathione, conjugation and one-carbon transcripts — OPLAH (− 1.24), GAMT (− 1.06), G6PD (− 0.70), CYP2A7 (− 0.61), ALDH1A3 (− 0.60), GSTZ1 (− 0.51), CYP26A1 (− 0.41), ALDH1L1 (− 0.39) and CBS (− 0.35) — together with TFRC (− 0.39), the copper chaperone ATOX1 (− 0.48), the zinc transporter SLC39A3 (− 0.34), the cGAS–STING-arm exonuclease TREX1 (− 0.46), the tight-junction protein cingulin (CGN, − 0.48), ubiquitin B (UBB, − 0.30) and the mitochondrial transcripts CYCS (− 0.52), TUFM (− 0.45) and FXN (− 0.22). The panel therefore records higher iron-storage and stress-response transcripts alongside lower transcripts for routine clearance and glutathione handling in the same tissue.

The meta-analysis was reproduced exactly from the three per-cohort GEO2R result tables (Methods; Supplementary Text S1): pooled log2 fold-changes, I^2, FDR status and high-confidence status agreed for all 442 genes with the locked results. For genes measured by several array probes, the locked analysis used the probe with the smallest P value; because that choice depends on the outcome, it departs from the rule-based construction of the panel. As a sensitivity analysis, collapsing such probes by their mean instead gave 86 FDR-significant and 32 high-confidence genes; 29 of the 30 locked high-confidence genes were retained (PECAM1 was not; FDR 0.14), all 30 kept the same direction, and pooled estimates under the two rules correlated at r = 0.978 (Data S1).

Sensitivity of the primary result

Panel genes did not change more often than other genes. Applied unchanged to all 19,365 genes measured in at least two of the three cohorts, the pipeline gave transcriptome-wide FDR < 0.05 for 76 of the 442 panel genes (17.2%) and 2,939 of the 18,923 other genes (15.5%; odds ratio 1.13, Fisher P = 0.35); 30 panel genes (6.8%) and 1,233 other genes (6.5%) met the high-confidence rule (P = 0.77), and 18% of 20,000 random sets of 442 measured genes had at least as many FDR-significant genes as the panel. All 30 high-confidence genes, and 76 of the 78 FDR-significant panel genes, kept their status under transcriptome-wide correction. None of the three cohorts showed a transcriptome-wide offset of the kind that excluded GSE131282 (median log2 fold-change − 0.02 to + 0.10; 45–54% of genes negative), but 46% of all measured genes reached nominal P < 0.05 in GSE138614 and 51% in GSE108000, against 2% in GSE32915 (Table S5). In the donor-level re-fit described below, the panel showed a slight excess (111 of 444 panel genes, 25.0%, against 4,074 of 19,348 other genes, 21.1%; odds ratio 1.25, P = 0.046). The white-matter signal is therefore broad, and the panel genes share in it rather than standing out clearly from it.

Allowing for repeated samples per donor. Each cohort was re-fitted with the donor or lesion as the unit: GSE138614 counts were summed per donor (10 MS and 5 control donors; PyDESeq2 with the GEO2R settings), GSE32915 values were averaged per patient (4 versus 4 controls; limma) and GSE108000 rim and perilesional values were averaged per lesion (15 lesions versus 10 controls; limma), and the locked pipeline was re-applied (Methods). The pooled estimates correlated closely with the locked ones (r = 0.93 across panel genes), all 30 high-confidence genes kept their direction and 29 remained FDR-significant, and 117 panel genes reached FDR < 0.05; but only 17 met the high-confidence rule: 12 of the locked 30 (AKR1C3, ALDH1A3, ALDH1L2, CP, CYP2A7, G6PD, GAMT, MGST2, OPLAH, PPARG, SLC7A11 and XBP1) and 5 others (ABCB1, CLDN12, CYP1B1, IFI16 and SULT1C2). HMOX1, FTL and PECAM1 remained FDR-significant (FDR 0.0002, 4×10^{-6} and 2×10^{-6}) but lost high-confidence status, because at donor level GSE138614 is nominally significant for 14 of the 30 genes rather than all 30. An approximate design-effect bound applied to the locked tables gave a similar reduction (16, 11, 8 and 6 high-confidence genes at within-donor correlations of 0.25, 0.5, 0.75 and 1; Table S4).

Adjusting for tissue composition. Adding a per-unit oligodendrocyte marker score (mean standardized expression of PLP1, MOG, MOBP, MBP, MAG and OPALIN) to the donor-level models left 64 FDR-significant panel genes and 9 high-confidence genes, of which GAMT, PPARG and ALDH1L2 are among the locked 30; adding a macrophage score (CD68, CD163 and CSF1R) as well left 21 and 4 (Table S4). All 30 locked genes kept their direction with the oligodendrocyte score. Because oligodendrocyte loss is itself part of MS pathology and the scores differ strongly between MS and control tissue, these models remove disease-related signal as well as composition; they show how much of the panel signal travels with cell-type change, not that the remainder is regulation within cells.

Choice of random-effects method. With three cohorts, the Hartung–Knapp–Sidik–Jonkman method tests the pooled estimate against a t distribution with 2 degrees of freedom (Methods). Under it no panel gene reached FDR < 0.05 (smallest P = 0.0006, HMOX1), although 23 of the 30 high-confidence genes had nominal P < 0.05. Per-gene inference from three cohorts therefore depends on the method chosen;

the DerSimonian–Laird result is reported as locked, and the agreement in direction across cohorts and in GSE123496 is the more robust evidence.

Independent-cohort check of the high-confidence set

GSE123496 contributed nothing to the locked meta-analysis. It comprises bulk RNA-seq of five brain regions (hippocampus, frontal cortex, internal capsule, corpus callosum and parietal cortex) from five MS donors and five controls (25). All 30 high-confidence genes were measured, and 25 of 30 (83%) changed in the same direction as the pooled estimate (exact binomial p = 0.0003, two-sided); the GSE123496 log2 fold-changes correlated with the pooled estimates (Pearson r = 0.73; Spearman ρ = 0.75, p = 1.9×10^{-6}; Fig. 2, Table S3). Concordance was 13 of 18 for genes lower in MS and 12 of 12 for genes higher in MS. Against a gene-label permutation baseline across all measurable panel genes, the 95th percentile of |r| was 0.35 and no permutation reached the observed correlation (p ≤ 0.0002, 5,000 permutations). The five discordant genes were all lower in the pooled estimate and higher in GSE123496: G6PD (+ 0.14), TUFM (+ 0.07), UBB (+ 0.18), CBS (+ 0.17) and ALDH1L1 (+ 0.81). Only ALDH1L1 was individually significant in the discordant direction (adjusted P = 0.019); it is an astrocyte-enriched transcript, and GSE123496 mixes grey- and white-matter regions. GSE123496 has a slight transcriptome-wide negative skew (60% of genes negative), and 55% of its measurable panel genes are positive; against the 49% concordance expected from that sign distribution, 25 of 30 remains significant (exact binomial P = 0.0002).

Lesion-stage analysis in GSE138614

The five GSE138614 lesion types were each compared with the 25 control white-matter samples (PyDESeq2 on the deposited counts; Methods; Supplementary Text S2). Samples were treated as independent, although the 73 MS samples come from 10 patients and the 25 control samples from 5 donors, so adjusted P values and hit counts are optimistic. Each lesion type comes from 4 to 7 donors (NAWM 7, active 7, chronic active 6, inactive 4, remyelinating 4), and 12 of the 14 inactive-lesion samples come from two donors. The originating authors' results, which account for patient, age and sex, are compared in Supplementary Text S2. Panel hits (FDR < 0.05 and |log2 fold-change| ≥ 0.5) numbered 15 in NAWM, 133 in active lesions, 99 in chronic active lesions, 114 in inactive lesions and 75 in remyelinating lesions (Table 2). Table 3 shows the stage pattern for 14 genes, selected for discussion after inspection of the results.

In NAWM — tissue without histological demyelination — 15 panel genes reached the hit criterion. Seven were higher: SULT1C2 (+ 1.36, adjusted P = 0.001), ABCC3 (+ 1.29, 0.019), CYP2S1 (+ 1.26, 0.004), ALDH1A2 (+ 1.15, 0.005), CP (+ 1.05, 0.006), ABCB1 (+ 0.95, 0.013) and SLC47A1 (+ 0.72, 0.037). Eight were lower: OSGIN1 (− 1.24, 0.046), MT1M (− 1.10, 0.005), MT2A (− 0.95, 0.026), MT1X (− 0.95, 0.042), MT1E (− 0.88, 0.032), NOS2 (− 0.81, 0.034), AOX1 (− 0.73, 0.012) and ME1 (− 0.56, 0.030). Four of the eight lower genes are metallothioneins. Composition data show an 11.1 percentage-point lower

oligodendrocyte fraction in NAWM than in control white matter, with modest astrocyte (+ 2.8 points) and endothelial/pericyte (+ 2.3 points) expansion (Table 4), so part of the NAWM signal may reflect cellular reorganization rather than per-cell change. In a donor-level re-fit (NAWM from 7 donors against 5 control donors) none of the 15, and no panel gene, met the hit criterion; in the originating authors' patient-adjusted results, 6 of the 14 they report reached FDR < 0.05 (SULT1C2, CP, ABCB1, SLC47A1, AOX1 and ME1). These NAWM hits are the least secure result in this paper.

Active lesions showed the largest number of hits (133). Among them were CP (+ 2.19, adjusted P = 3.5×10^{-13}), PPARG (+ 1.49, 1.1×10^{-8}), VCAM1 (+ 1.68, 3.3×10^{-4}), CLDN5 (+ 2.26, 9.7×10^{-4}) and HMOX1 (+ 1.40, 0.0015), with lower GPX4 (− 0.58, 0.026) and CLDN11 (− 0.96, 3.5×10^{-5}). HMOX1 was FDR-significant in active (adjusted P = 0.0015) and inactive lesions (+ 1.52, 0.0028), nominally higher in remyelinating lesions (P = 0.019), and not changed in chronic active lesions or NAWM. GPX4 was lower in active, inactive (− 0.75, adjusted P = 0.0024) and remyelinating lesions (− 1.08, 0.033) and not in chronic active lesions or NAWM. CP, ABCB1, PPARG, PECAM1, NDUFS2 and CLDN11 changed in four or five lesion types (Table 3).

Table 2

GSE138614: panel hits by lesion type against control white matter. PyDESeq2 on the deposited count matrix, each lesion type against the 25 control white-matter samples; samples were treated as independent (73 MS samples from 10 patients; 25 control samples from 5 donors); the number of MS donors in each group is given in parentheses. Hit = Benjamini–Hochberg adjusted $P < 0.05$ and $|\log2 \text{ fold-change}| \geq 0.5$. "Panel genes tested" = panel genes with an adjusted P in that contrast (after independent filtering). Percentages are of the full panel (468) and of the genes tested. Leading hits are listed in order of adjusted P; ↑ higher, ↓ lower in the lesion type. Per-gene values are in Data S2. These single-contrast counts are descriptive; the three-cohort meta-analysis is the primary inferential result.

Comparison	n (MS)	n (control)	Panel genes tested	Hits	Up / down	Hits (% panel / % tested)	Leading hits
NAWM vs control WM	21 (7)	25	398	15	7 / 8	3.2% / 3.8%	SULT1C2↑, CYP2S1↑, ALDH1A2↑, MT1M↓, CP↑, AOX1↓, ABCB1↑, ABCC3↑
Active lesion vs control WM	16 (7)	25	418	133	94 / 39	28.4% / 31.8%	SULT1C2↑, CP↑, GPX8↑, ABCC3↑, CDH1↓, GPX3↑, SLC47A1↑, JAM3↓
Chronic active lesion vs control WM	17 (6)	25	417	99	53 / 46	21.2% / 23.7%	CP↑, RARB↑, GPX8↑, GCLC↓, AOX1↓, JAM3↓, ALDH1A1↓, CYP1B1↑
Inactive lesion vs control WM	14 (4)	25	417	114	60 / 54	24.4% / 27.3%	CDH1↓, ALDH1A1↓, GCLC↓, GPX8↑, ABCC3↑, SULT1C2↑, CP↑, IDH2↓
Remyelinating lesion vs control WM	5 (4)	25	423	75	38 / 37	16.0% / 17.7%	TF↓, PAPSS1↓, NDUFS2↓, SULT1C2↑, JAM3↓, ABCB11↑, GPX8↑, SLC30A1↑

Table 3

GSE138614: stage pattern of 14 panel genes discussed in the text. Each lesion type against the 25 control white-matter samples (PyDESeq2). ↑/↓ direction; ** adjusted P < 0.05; *** adjusted P < 0.01; nom = nominal P < 0.05 with adjusted P ≥ 0.05; — = P ≥ 0.05. NAWM, normal-appearing white matter; AL, active; CA, chronic active; IL, inactive; RL, remyelinating lesion.

Gene	NAWM	AL	CA	IL	RL	Function
CP	↑***	↑***	↑***	↑***	↑***	Iron/copper; ferroxidase
ABCB1	↑**	↑***	↑***	↑***	↑***	Efflux transporter (P-glycoprotein)
PPARG	nom ↑	↑***	↑***	↑***	↑**	Nuclear receptor
PECAM1	nom ↑	↑***	↑**	↑***	↑***	Endothelial adhesion
VCAM1	—	↑***	nom ↑	nom ↑	nom ↑	Endothelial/immune adhesion
HMOX1	—	↑***	—	↑***	nom ↑	Heme degradation; NRF2 target
NQO1	—	↑***	—	↑**	↑**	NRF2 target
CLDN5	—	↑***	—	—	—	Endothelial tight junction
CYP2A6	nom ↓	↓***	↓***	↓**	↓**	Cytochrome P450
CLDN11	—	↓***	↓**	↓***	↓***	Oligodendrocyte myelin claudin
NDUFS2	—	↓***	↓***	↓***	↓***	Complex I subunit
GPX4	—	↓**	—	↓***	↓**	Phospholipid glutathione peroxidase
MT1E	↓**	nom ↓	↓**	↓***	nom ↓	Metallothionein
AQP1	—	nom ↓	↓***	↓***	nom ↓	Water channel

Cell-type composition (Macnair et al.)

Cell-level metadata from a separate single-nucleus atlas of MS and control brain tissue (24) provided composition context for the bulk signals. The atlas samples are not the tissue profiled in the bulk cohorts, so its fractions indicate the direction and approximate size of composition shifts by lesion type, not the composition of the bulk samples. Control white matter is 75.2% oligodendrocytes, 8.5% microglia and 5.7% astrocytes (Table 4). Active lesions showed the largest shift: oligodendrocytes fell to 43.9% (− 31.3 points), microglia rose to 14.9% (+ 6.4) and astrocytes to 15.1% (+ 9.4). NAWM showed a smaller shift (− 11.1 points oligodendrocytes, + 2.8 points astrocytes). This analysis quantifies composition only; it is not differential expression within cell types. The bulk cohorts show the same shift: four of six oligodendrocyte marker transcripts (MOG, MOBP, MBP and MAG) were lower in all three meta-analyzed cohorts, whereas PLP1 was not lower in GSE32915 or GSE108000 and OPALIN not in GSE32915 (Table S6) (for example MOG − 1.04, − 0.87 and − 0.76, and MAG − 1.36, − 0.76 and − 1.13 log2 units in GSE138614, GSE32915 and GSE108000), GFAP was higher in all three (+ 0.82, + 0.54 and + 0.88), and the

macrophage transcripts CD68 and CD163 were higher in GSE138614 (+ 1.20, + 2.45) and GSE108000 (+ 1.03, + 0.88) (Table S6).

Table 4

Cell-type composition of MS white matter by lesion type (Macnair et al.; Zenodo 8338963). Values are percentages of white-matter nuclei; changes from control white matter in percentage points in parentheses. Data source: ms_lesions_snRNAseq_col_data_2023-09-12.txt; 335,694 white-matter nuclei of 632,375 in the atlas (control white matter 54,721; NAWM 60,059; active 76,268; chronic active 60,958; inactive 39,822; remyelinating 43,866). Rows do not sum to 100%: the remaining nuclei are neurons (5.1% of control white matter; 10.8%, 18.1%, 10.8%, 11.7% and 8.0% in NAWM, active, chronic active, inactive and remyelinating lesions) and B and T lymphocytes (0.1% to 1.2%). OPCs, oligodendrocyte precursor cells; COPs, committed oligodendrocyte precursors.

Cell type	Control WM	NAWM	Active	Chronic active	Inactive	Remyelinating
Oligodendrocytes	75.2%	64.1% (− 11.1)	43.9% (− 31.3)	50.7% (− 24.5)	52.8% (− 22.4)	60.8% (− 14.4)
Microglia	8.5%	8.8% (+ 0.3)	14.9% (+ 6.4)	16.2% (+ 7.7)	11.7% (+ 3.2)	9.8% (+ 1.3)
Astrocytes	5.7%	8.5% (+ 2.8)	15.1% (+ 9.4)	15.1% (+ 9.4)	16.4% (+ 10.7)	14.5% (+ 8.8)
OPCs + COPs	4.5%	4.1% (− 0.4)	4.3% (− 0.2)	3.4% (− 1.1)	3.2% (− 1.3)	3.1% (− 1.4)
Endothelium + pericytes	0.8%	3.1% (+ 2.3)	2.7% (+ 1.9)	2.7% (+ 1.9)	3.1% (+ 2.3)	2.8% (+ 2.0)

Composition bears directly on two recurrent signals. GPX4 is expressed abundantly by oligodendrocytes, and the oligodendrocyte fraction falls by 14 to 31 points in the lesion types where GPX4 is lower; cell loss alone could therefore produce the bulk decrease, and per-cell suppression in surviving oligodendrocytes cannot be separated from it on these data. CLDN11, an oligodendrocyte myelin claudin, falls in the same lesion types and serves as an internal marker of oligodendrocyte depletion. HMOX1 rises in lesion types where microglia and astrocytes expand, so its bulk increase is compatible with expansion of those compartments, with or without per-cell induction. CP rises by + 1.9 to + 2.2 log2 units across the four demyelinated lesion types, more than the roughly 1.4 log2 units that a 5.7% to 15.1% astrocyte fraction alone would produce if CP were confined to astrocytes; this suggests, but does not show, per-cell induction. The same consideration applies to the primary high-confidence set: several of its higher transcripts, including HMOX1, PPARG and PECAM1, are expressed mainly by microglia, macrophages or endothelial cells, compartments that expand in lesions. Chronic active lesions are a partial counter-example: their oligodendrocyte fall (− 24.5 points) and microglial and astrocytic expansion (+ 7.7 and + 9.4 points) are comparable to those of inactive lesions, yet neither GPX4 nor HMOX1 changed in them (Table 3), so composition is unlikely to be the whole explanation. Whether each high-confidence gene is enriched in a cell type whose fraction changes was not tested, and no composition adjustment was applied to the meta-analysis.

Lesion-zone and grey-matter tiers

Table 5 summarizes all datasets. In GSE108000, each lesion zone was compared with the 10 control white-matter samples. Panel hits were 105 (24.1%) in the rim of chronic active lesions, 94 (21.6%) in the perilesional zone of chronic active lesions, 85 (19.5%) in the rim of inactive lesions and 94 (21.6%) in the perilesional zone of inactive lesions. CP was higher in all four zones (+ 1.64 to + 2.24). HMOX1 was FDR-significant in the rim of chronic active lesions (+ 1.61, adjusted $P = 1.1 \times 10^{-5}$), the rim of inactive lesions (+ 0.83, 0.019) and the perilesional zone of chronic active lesions (+ 0.64, 0.047), but not in the perilesional zone of inactive lesions; it was strongest at the chronic active rim. GPX4 was lower in the perilesional zone of chronic active lesions (− 0.84, 0.0078), the rim of inactive lesions (− 0.86, 0.0016) and the perilesional zone of inactive lesions (− 1.02, 0.0002), and nominally lower at the chronic active rim. NDUFS2 was lower and PECAM1 higher in all four zones.

In cortical grey matter (GSE135511; each group of 10 against the same 10 controls), follicle-negative grey-matter lesions showed 62 panel hits (16.8% of 370 measurable) and follicle-negative normal-appearing grey matter 60 (16.1% of 373), against 2 (0.5% of 373; GSTM1 and GSTM2, both lower) in follicle-positive grey-matter lesions. HMOX1 (+ 1.46 and + 1.44), AQP1 (+ 1.65 and + 1.77), CLDN5 (+ 0.81 and + 0.88) and NQO1 (+ 1.13 and + 1.17) were higher, and GPX4 (− 0.43 and − 0.39) and NDUFS2 lower, in follicle-negative lesions and normal-appearing grey matter respectively. The two follicle-negative contrasts come from the same 10 donors and share the control group, so they are not independent observations. Re-analyzed from the series matrix, follicle-positive normal-appearing grey matter (GSM4013340–GSM4013349), the fifth group in the series, showed 5 panel hits (1.3% of 371 measurable; GSTM1, GSTM2, GSTM4, PRDX2 and USP14, all lower) against the same controls. A direct comparison of follicle-negative with follicle-positive lesions (10 donors each) found no gene at FDR < 0.05 anywhere in the transcriptome, and neither did the corresponding comparison of normal-appearing grey matter. In the follicle-negative lesion contrast, re-analyzed from the series matrix with gene-level Benjamini–Hochberg correction (63 hits among 366 measurable panel genes, against 62 of 370 in the GEO2R table above), panel genes were hits at the same rate as all measured genes (17.2% and 17.6%; Data S4). In GSE131279, a within-MS comparison of 37 cortical grey-matter lesion samples from 18 donors with 41 normal-appearing grey-matter samples from 20 donors (samples treated as independent), 18 of 448 measurable panel genes (4.0%) were hits, including lower MT1A and CLDN11 and higher CYP2D6 and UGT1A6.

Table 5

Datasets, panel coverage and single-contrast panel hits. Hits = panel genes with Benjamini–Hochberg adjusted P < 0.05 and |log2 fold-change| ≥ 0.5 in that contrast (GEO2R; lowest-P probe per gene), as a percentage of measurable panel genes; GSE138614 lesion-type hits are from the PyDESeq2 re-analysis (Table 2), and its panel coverage (386) is that of the GEO2R table used in the meta-analysis. Key genes: ↑/↓ FDR-significant; nom = nominal P < 0.05 only. WM, white matter; GM, grey matter; NAGM, normal-appearing grey matter; HC, high-confidence. The per-gene values for every contrast are in Data S3. Only GSE138614, GSE32915 and GSE108000 enter the meta-analysis; all other rows are supporting tiers or checks and are not pooled. n is given in samples, with donors or lesions where the public record states them (GSE138614: 72 MS samples in the NCBI-generated counts used by GEO2R; the lesion-type re-analysis uses all 73 in the authors' count matrix); in every contrast, samples from the same donor or lesion were treated as independent.

Dataset	Platform	Comparison	n (MS / control)	Panel genes	Hits	Key genes / role
GSE138614	RNA-seq (GPL21697)	NAWM and WM lesions (4 types) vs control WM	72 / 25 (10 / 5 donors)	386	Meta cohort; lesion-type hits 15–133 (Table 2)	Locked meta-analysis; lesion-stage tier
GSE32915	Agilent (GPL4133)	Acute MS NAWM and lesion areas vs control WM	12 (4 patients) / 4	435	0	Locked meta-analysis
GSE108000	Agilent (GPL13497)	All lesion-zone samples (15 lesions) vs control WM	30 / 10	436	Meta cohort	Locked meta-analysis
GSE108000	Agilent (GPL13497)	Rim, chronic active vs control WM	7 / 10	436	105 (24.1%)	CP↑, HMOX1↑, GPX4 nom ↓, PPARG↑, NDUFS2↓, PECAM1↑
GSE108000	Agilent (GPL13497)	Perilesion, chronic active vs control WM	7 / 10	436	94 (21.6%)	CP↑, HMOX1↑, GPX4↓, PPARG↑, NDUFS2↓, PECAM1↑
GSE108000	Agilent (GPL13497)	Rim, inactive vs control WM	8 / 10	436	85 (19.5%)	CP↑, HMOX1↑, GPX4↓, PPARG↑, NDUFS2↓, PECAM1↑
GSE108000	Agilent (GPL13497)	Perilesion, inactive vs control WM	8 / 10	436	94 (21.6%)	CP↑, GPX4↓, PPARG↑, NDUFS2↓, PECAM1↑

Dataset	Platform	Comparison	n (MS / control)	Panel genes	Hits	Key genes / role
GSE135511	Illumina (GPL6883)	GM lesion, follicle-negative vs control GM	10 / 10	370	62 (16.8%)	HMOX1↑, AQP1↑, CLDN5↑, NQO1↑, GPX4↓, NDUFS2↓, GSTM1↓, GSTM2↓
GSE135511	Illumina (GPL6883)	NAGM, follicle-negative vs control GM	10 / 10	373	60 (16.1%)	HMOX1↑, AQP1↑, CLDN5↑, NQO1↑, GPX4↓, NDUFS2↓, GSTM1↓, GSTM2↓
GSE135511	Illumina (GPL6883)	GM lesion, follicle-positive vs control GM	10 / 10	373	2 (0.5%)	HMOX1 nom ↑, NQO1 nom ↑, NDUFS2 nom ↓, GSTM1↓, GSTM2↓
GSE135511	Illumina (GPL6883)	NAGM, follicle-positive vs control GM	10 / 10	371	5 (1.3%)	GSTM1↓, GSTM2↓, GSTM4↓, PRDX2↓, USP14↓; re-analysis from series matrix
GSE135511	Illumina (GPL6883)	GM lesion, follicle-negative vs follicle-positive	10 / 10	370	0	Direct contrast; no gene at FDR < 0.05 transcriptome-wide
GSE131279	Illumina (GPL10558)	GM lesion vs NAGM, within MS	37 lesion / 41 NAGM (within MS)	448	18 (4.0%)	MT1A↓, CLDN11↓, CYP2D6↑, UGT1A6↑
GSE123496	RNA-seq (GPL21290)	Five brain regions, MS vs control	5 donors / 5 donors (25 / 25 samples)	30 of 30 HC	—	Independent check of the high-confidence set (Fig. 2)
Macnair et al.	snRNA-seq metadata	WM lesion types; composition only	335,694 WM nuclei	—	—	Cell-type fractions (Table 4)
GSE131282	Illumina (GPL10558)	GM, MS vs control	142 / 42 (49 donors)	452	—	Excluded: offset from separately

Dataset	Platform	Comparison	n (MS / control)	Panel genes	Hits	Key genes / role
						normalized sub-series (Fig. 3)
GSE131281	Illumina (GPL10558)	NAGM vs control GM (sub-series of GSE131282)	64 / 42 (25 / 14 donors)	452	1 (0.2%)	GSTM5↑; 10 panel genes at FDR < 0.05; none at donor level (Fig. 3C)
GSE38010	Affymetrix (GPL570)	Brain plaques vs control	5 / 2	—	—	Excluded: non-log-transformed values
GSE52139	Affymetrix (GPL570)	Spinal cord periplaque vs NAWM, within MS	no control	—	—	Excluded: no non-MS control

Cross-tier concordance

Table 6 follows selected panel genes across the four supporting datasets. CP was higher in all five GSE138614 lesion types and all four GSE108000 zones and nominally higher in follicle-negative grey matter. NDUFS2 was lower and PECAM1 higher in GSE138614, GSE108000 and the follicle-negative GSE135511 contrasts, and neither changed in GSE131279. GPX4 was lower in three GSE138614 lesion types, three GSE108000 zones and both follicle-negative grey-matter contrasts. HMOX1 was higher in two GSE138614 lesion types, three GSE108000 zones and both follicle-negative grey-matter contrasts. AQP1 differed in direction by tissue: lower in chronic active and inactive white-matter lesions, higher in follicle-negative grey matter. ACSL4 and MT1A, frequently discussed in the ferroptosis and metallothionein literature, showed no consistent change: ACSL4 was unchanged in all five GSE138614 lesion types, higher only in the perilesional zone of chronic active lesions, and lower in follicle-negative grey matter; MT1A was unchanged in white matter and lower only in GSE131279. These supporting contrasts are not independent replications: the GSE138614 lesion types share donors and controls, the GSE108000 zones share lesions and controls, and the two follicle-negative GSE135511 contrasts share donors and controls, so the cross-tier pattern rests on four datasets rather than on thirteen independent contrasts. The genes in Tables 3 and 6 were selected for discussion after the results were inspected.

Table 6

Selected panel genes across the supporting datasets. ↑/↓ = Benjamini–Hochberg adjusted P < 0.05 in the listed contrasts; nom = nominal P < 0.05 only; — = no contrast with P < 0.05; not measured = gene absent from that platform. GSE138614: lesion types vs control WM (AL, active; CA, chronic active; IL, inactive; RL, remyelinating). GSE108000: rim and perilesional (peri) zones of chronic active (CA) and inactive (IL) lesions vs control WM. GSE135511: follicle-negative (FN) and follicle-positive (FP) grey-matter lesions and FN normal-appearing grey matter (NAGM) vs control GM. GSE131279: GM lesion vs NAGM within MS. ACSL4 and MT1A are shown because they are prominent in the ferroptosis and metallothionein literature; neither changes consistently here. Genes were selected for display after inspection of the results.

Gene	GSE138614 (WM lesion types)	GSE108000 (WM lesion zones)	GSE135511 (cortical GM)	GSE131279 (GM, within MS)
CP	↑ NAWM, AL, CA, IL, RL	↑ rim-CA, peri-CA, rim-IL, peri-IL	nom ↑ FN lesion, FN NAGM	—
PECAM1	↑ AL, CA, IL, RL; nom ↑ NAWM	↑ rim-CA, peri-CA, rim-IL, peri-IL	↑ FN lesion, FN NAGM	—
NDUFS2	↓ AL, CA, IL, RL	↓ rim-CA, peri-CA, rim-IL, peri-IL	↓ FN lesion, FN NAGM; nom ↓ FP lesion	—
PPARG	↑ AL, CA, IL, RL; nom ↑ NAWM	↑ rim-CA, peri-CA, rim-IL, peri-IL	nom ↑ FP lesion	nom ↓ lesion vs NAGM
HMOX1	↑ AL, IL; nom ↑ RL	↑ rim-CA, peri-CA, rim-IL	↑ FN lesion, FN NAGM; nom ↑ FP lesion	—
GPX4	↓ AL, IL, RL	↓ peri-CA, rim-IL, peri-IL; nom ↓ rim-CA	↓ FN lesion, FN NAGM	—
NQO1	↑ AL, IL, RL	not measured	↑ FN lesion, FN NAGM; nom ↑ FP lesion	nom ↑ lesion vs NAGM
CLDN11	↓ AL, CA, IL, RL	—	not measured	↓ lesion vs NAGM
AQP1	↓ CA, IL; nom ↓ AL, RL	nom ↑ rim-CA	↑ FN lesion, FN NAGM	—
MT1E	↓ NAWM, CA, IL; nom ↓ AL, RL	—	—	—
ACSL4	—	↑ peri-CA	↓ FN lesion, FN NAGM; nom ↓ FP lesion	nom ↓ lesion vs NAGM
MT1A	—	—	—	↓ lesion vs NAGM

Exclusion of the grey-matter SuperSeries GSE131282

The grey-matter SuperSeries GSE131282 (142 MS versus 42 control cortical grey-matter samples) was assessed as a candidate comparator and is not usable as one. Re-analyzed from its two sub-series with probes mapped through the annotation of its own platform (GPL10558; Methods), 31,149 of 31,334 genes (99.4%) carry a negative log2 fold-change; 91.0% reach FDR < 0.05, and 99.9% of those are lower in MS. The median log2 fold-change of the whole transcriptome is − 0.29 and its 99th percentile is − 0.02 (Fig. 3A). A shift of that shape reflects a difference in scale between the two arms rather than a biological result. Panel genes share the shift and are shifted further than other genes (439 of 452 panel genes at FDR < 0.05 against 28,080 of 30,882 others; median log2 fold-change − 0.48 against − 0.29). Only 24 genes are FDR-significant and positive, headed by HLA-DRB5 (+ 1.78) and HLA-DRB1 (+ 1.49), the finding reported by the originating study (23); effects large enough to clear the offset remain visible, while effects of ordinary magnitude are buried beneath it (Fig. 3B). The offset has a technical source. GSE131282 is a SuperSeries of two sub-series that were normalized separately: every sample of GSE131279, which compares lesion with normal-appearing grey matter within MS and is used above as a supporting contrast, has a log2 median of 7.96, and every sample of GSE131281, which compares normal-appearing grey matter with control grey matter, has a median of 8.65. All 42 control samples are in GSE131281, whereas 78 of the 142 MS samples are in GSE131279, so pooling the sub-series places a normalization difference between MS and control tissue. The series metadata show a second, independent problem: the 184 samples come from 49 donors (35 MS, 14 control), with a median of three tissue blocks per donor and one donor contributing 19, so a sample-level comparison understates its standard errors, a limitation that every cohort here shares to some degree (Limitations). GSE131282 is excluded as a pooled series because of the scale offset; the pseudoreplication is a further caveat. Within GSE131281 alone (64 normal-appearing grey-matter samples from 25 MS donors against 42 control samples from 14 donors, under one normalization) there is no offset (median log2 fold-change + 0.01; 46% of genes negative; Fig. 3C), and differential expression is sparse: 474 genes (1.5%) reach FDR < 0.05, including 10 panel genes, of which one (GSTM5, + 0.65) meets the hit criterion, and no gene remains at FDR < 0.05 when samples are averaged per donor (25 versus 14). HMOX1 (+ 0.16), GPX4 (− 0.05) and CP (− 0.13) are unchanged in this normal-appearing grey matter, and 20 of the 30 high-confidence genes change in the same direction as in white matter (binomial P = 0.10; Data S4).

Discussion

This paper reports a locked three-cohort white-matter meta-analysis of a pre-specified 468-gene panel in MS, its reproduction from the per-cohort GEO2R result tables, a check of its high-confidence set in an independent cohort, and supporting lesion-stage, lesion-zone, grey-matter and composition analyses. The 30 high-confidence associations reproduce exactly and move largely in the same direction in GSE123496, although their per-gene P values are optimistic because samples from the same donor were treated as independent. The set is not specific to the panel, whose genes change little more often than other genes, and re-fitted with the donor as the unit only 12 of the 30 remain high-confidence. Three transcript-level observations organize the supporting tiers: (i) higher CP in every white-matter lesion type and zone, and higher HMOX1, concentrated in active and inactive lesions and strongest at the chronic

active rim; (ii) lower GPX4 in lesion types that have lost oligodendrocytes; and (iii) 15 panel genes, four of them metallothioneins, already changed in NAWM, although none did so at donor level.

HMOX1: lesion stage, lesion zone and composition

HMOX1 transcript was higher in active and inactive white-matter lesions, in three of four GSE108000 lesion zones with the largest change at the chronic active rim, and in follicle-negative cortical grey matter. In the donor-level re-fit of the white-matter meta-analysis, HMOX1 remained FDR-significant (FDR 0.0002) but was no longer high-confidence (Table S4). Iron accumulates at the rims of chronic active lesions, and such rims predict clinical worsening (26–28). HMOX1 degrades heme to carbon monoxide, biliverdin and ferrous iron (29–31); acutely this can be protective, whereas sustained activity in an iron-laden environment could add to the ferrous iron pool. The present data cannot distinguish these possibilities. Composition data show that microglia and astrocytes expand in the lesion types where HMOX1 rises, so part of the bulk signal may be compositional. The measurements are transcript abundance only; they do not establish whether the response is beneficial or harmful.

GPX4 and the ferroptosis literature

Lower GPX4 transcript abundance recurred in three of five white-matter lesion types, three of four GSE108000 zones and both follicle-negative grey-matter contrasts, although GPX4 was not FDR-significant in the primary meta-analysis (pooled log2 fold-change − 0.40, FDR 0.34). In white matter this is compatible with two processes that the composition data cannot separate: oligodendrocyte depletion (a 31.3-point fall in oligodendrocyte fraction in active lesions) and lower expression within surviving oligodendrocytes. Neither amounts to a demonstration of ferroptosis, which was not assayed. ACSL4, whose product supplies the oxidizable phospholipids on which ferroptosis depends, was not higher in any GSE138614 lesion type, was higher only in the perilesional zone of chronic active lesions in GSE108000, and was lower in follicle-negative grey matter, so these data do not support a paired ACSL4-up, GPX4-down ferroptosis signature. Ferroptosis in MS and its models (11–13), the STING–GPX4 mechanism described in myocardium (16), STING signalling in MS and other neurodegenerative disease (17, 18, 32), and the report that dimethyl fumarate prevents ferroptosis through NRF2 in another organ (33) are cited as context; none was tested here. Testing a ferroptosis contribution would require within-cell-type differential expression, lipid-peroxidation measurement and rescue experiments.

Metallothioneins in normal-appearing white matter

Four metallothionein transcripts (MT1E, MT1M, MT1X and MT2A) were lower in NAWM, and MT1E remained lower in chronic active and inactive lesions. None of the four reached significance in the donor-level re-fit or in the originating authors' patient-adjusted NAWM results, so this observation is tentative. Decreased metallothionein-3 has been reported in MS and ALS spinal cord (34), but that study assayed a different isoform, and the present data are bulk measurements without cell-type resolution. Whether the lower metallothionein transcripts reflect per-cell change or composition cannot be decided from these data.

Cross-disease comparison

Cross-disease comparison is a descriptive comparison of gene symbols across separately conducted meta-analyses, not a pooled analysis, and the deposited per-disease results are less uniform than a single convergent pattern would suggest. Among glutathione-system genes, GSS is lower at FDR < 0.05 in Alzheimer's disease (− 0.30, high-confidence), Parkinson disease (− 0.62, high-confidence) and MS white matter (− 0.42); GSR is lower at FDR < 0.05 in Alzheimer's and Parkinson disease but not in MS white matter; and GPX4 is FDR-significant in Alzheimer's disease alone (− 0.18), with the MS white-matter pooled estimate of − 0.40 not reaching FDR significance (FDR 0.34). On the NRF2 axis, HMOX1 is high-confidence and higher in MS white matter (+ 0.88), Parkinson disease (+ 0.66) and ALS (+ 0.34), and FDR-significant but not high-confidence in Alzheimer's disease (+ 0.18), whereas NFE2L2 itself is high-confidence and higher in Parkinson disease (+ 0.50), higher but not FDR-significant in ALS (+ 0.30, FDR 0.06), and unchanged in MS white matter (− 0.04, FDR 0.88). Barrier genes do not converge: CLDN5 is higher in the Alzheimer's pooled estimate (+ 0.31, FDR 0.02) and in Parkinson disease (+ 0.35, FDR 0.04), not FDR-significant in ALS, and unchanged in MS white matter (− 0.12, FDR 0.95); the barrier-associated MS finding is CLDN11 (− 0.52, FDR 0.046), the oligodendrocyte myelin claudin, which tracks oligodendrocyte depletion rather than endothelial barrier loss. Per-gene values for every disease are in the locked per-disease results deposited at Zenodo (8), and the companion manuscripts (35–38) report them in full; the ALS values given here are from the donor-resolved ALS analysis (37), which supersedes the deposited ALS results.

Follicle stratification

Follicle-negative cortical lesions and follicle-negative normal-appearing grey matter each showed about 60 panel hits, whereas follicle-positive lesions from the same series, compared with the same controls on the same platform, showed two. The two follicle-negative contrasts come from the same donors, a difference in hit counts is not a test of a difference between groups, and a direct follicle-negative versus follicle-positive comparison found no gene at FDR < 0.05, in lesions or in normal-appearing grey matter, so the observation is descriptive and does not establish a follicle-dependent difference in any gene. Meningeal follicle-like structures are associated with more severe cortical pathology in progressive MS (39). The difference in hit counts is unexpected and has no explanation in these data. One possibility is that an immune-dominated transcriptional signature in follicle-positive tissue dilutes the glial and neuronal detoxification signal, which may be more prominent where intrinsic oxidative stress predominates (40, 41). Group sizes are 10 per group, and the finding needs replication.

Research implications

Anti-ferroptotic and NRF2-directed compounds appear in the cited literature. They are not assigned as treatments from these transcript contrasts. Cell-type-resolved differential expression, protein and activity measurements, and iron and lipid-peroxidation assays would be required before any targeting claim.

Limitations

All analyses use cross-sectional postmortem bulk tissue, so causal attribution and longitudinal dynamics are out of reach. Every cohort contributes more than one sample per donor or lesion: GSE138614 (73 MS samples from 10 patients; 25 control samples from 5 donors), GSE32915 (12 MS samples from four patients), GSE108000 (rim and perilesional pairs from 15 lesions), GSE135511 (lesion and normal-appearing grey matter from the same donors), GSE131279 (78 samples from 18 and 20 MS donors), GSE131281 (64 MS and 42 control samples from 25 and 14 donors) and GSE123496 (five regions from each of ten donors). Every contrast treated samples as independent, without blocking by donor or lesion, so per-gene P values, FDR counts, single-contrast hit counts and the per-cohort nominal-significance counts used by the high-confidence rule are optimistic; the direction-and-correlation check of the high-confidence set is made across genes rather than samples and is less affected. Re-fitted with the donor or lesion as the unit, the high-confidence set falls to 17 genes (12 of the original 30); GSE123496 and the supporting-tier contrasts other than NAWM were not re-fitted in this way. No contrast was adjusted for age, sex, postmortem interval or RNA quality. With three cohorts, the DerSimonian–Laird estimator can understate between-cohort variance, and I^2 is imprecise; under the Hartung–Knapp–Sidik–Jonkman method no gene reaches FDR < 0.05. Panel genes changed little more often than other genes (not significantly in the locked analysis; odds ratio 1.25, P = 0.046 at donor level), so the results describe panel genes within a broad white-matter signal and do not show that the panel is specifically involved in MS. The composition analysis addresses cell-type fractions only, comes from a separate single-nucleus study, and was not used to adjust the bulk estimates (adjustment of the donor-level models for an oligodendrocyte marker score leaves 9 high-confidence genes, but also removes disease-related signal); within-cell-type (pseudobulk) differential expression requires the full count matrix of the atlas and was not performed. The three meta-analyzed cohorts differ in platform and design: GSE32915 samples acute MS, GSE138614 progressive MS, and GSE108000 chronic active and inactive lesions. GSE138614 (UK Multiple Sclerosis Society Tissue Bank) and GSE108000 (Netherlands Brain Bank) come from different brain banks, so donor overlap between them is unlikely. GSE123496 mixes grey and white matter, so it is a check of direction in brain tissue, not a white-matter replication. For array genes measured by several probes the locked analysis used the probe with the smallest P value, a choice that depends on the outcome; the mean-probe sensitivity analysis retained 29 of 30 high-confidence genes. The genes discussed from the supporting tiers (Tables 3 and 6) were selected after inspection of the results. The cortical grey-matter evidence is weaker than the white-matter evidence: the largest grey-matter series was excluded as pooled because its separately normalized sub-series create a scale offset (Fig. 3); its control-containing sub-series (GSE131281) shows little differential expression in normal-appearing grey matter, and what remains is a small follicle-stratified series (GSE135511) and a within-MS contrast without controls (GSE131279). The panel was curated by functional-family enumeration from biological rationale rather than data-driven selection, and its transcript-level findings do not measure enzyme activity, iron content or lipid peroxidation.

Conclusion

A locked three-cohort white-matter meta-analysis identifies 30 high-confidence panel-gene associations in MS: higher iron-storage and stress-response transcripts alongside lower glutathione, conjugation and one-carbon transcripts. The result reproduces exactly from the per-cohort result tables and is largely concordant in an independent cohort, although per-gene P values are optimistic because samples from the same donor were treated as independent, and part of the pattern may reflect tissue composition. Panel genes change little more often than other genes, the high-confidence set falls to 17 (12 of the original 30) when re-fitted with the donor as the unit, and no gene reaches FDR < 0.05 under a Hartung–Knapp–Sidik–Jonkman test, so the findings are best read as a description of panel genes within a broad white-matter signal. Across supporting tiers, higher HMOX1 transcript is concentrated in active and inactive lesions and strongest at the chronic active rim, and lower GPX4 transcript accompanies oligodendrocyte loss; both are bulk observations that composition shifts may partly explain, and neither demonstrates ferroptosis. Dimethyl fumarate is an approved NRF2-pathway drug in relapsing MS; that clinical fact is background pharmacology and not validation of this panel, this analysis, or any treatment inference from it.

Materials and Methods

The 468-gene panel

Analyses use the locked 468-gene panel (MASTER_panel_FINAL_v468_7.5.26, frozen 5 July 2026) of the methods-and-panel manuscript (1), deposited at Zenodo together with the excluded-symbol list and the analysis pipeline (8). The panel comprises 394 core detoxification, antioxidant, metal and barrier genes, 12 core cGAS–STING genes, 10 core ferroptosis/iron/NRF2 completeness genes, 40 broader cellular-defence genes and 12 genes of a placental/sex-steroid module (labelled 'ASD-maternal module' in the frozen panel file); the tiers are partitions of one panel, and all 468 genes enter every analysis. The panel originates in the detoxification panel of the foundation study (6). Pseudogenes and ambiguous symbols were removed by rule, and panel membership was set by functional-family rules. The MS cohort screen (27 June 2026; Table S1) preceded the panel freeze (5 July 2026), at which ten genes were added (AIFM2, CUL3, FXN, GCH1, GLO1, HAGH, MFSD2A, RBX1, TF and TFRC); two of them, FXN and TFRC, are among the 30 high-confidence genes reported here. Excluding all ten gives 432 meta-analyzable, 75 FDR-significant and 28 high-confidence genes, the locked set without FXN and TFRC (Table S4).

Cohorts

GSE138614 (19) comprises 98 white-matter samples (Illumina NextSeq 550, GPL21697) from 10 patients with progressive MS and 5 control donors, supplied by the UK Multiple Sclerosis Society Tissue Bank (donor labels in the GEO sample annotations; 4–11 samples per MS donor and 5 per control donor): 25 control white matter, 21 NAWM, 16 active, 17 chronic active, 14 inactive and 5 remyelinating lesions (group sizes from the GEO sample annotations; the original publication reports 19, 18, 17, 13 and 6 for the MS groups). GEO records its counts as STAR alignment followed by HTSeq-count. GSE32915 (20) (Agilent 4x44K, GPL4133) comprises 16 samples: 12 samples of NAWM, initial-lesion and early

demyelinated areas from four patients with acute MS (GSM814820–GSM814827 and GSM1236642–GSM1236645) and white matter from four controls (GSM814828–GSM814831). GSE108000 (21) (Agilent SurePrint G3, GPL13497) comprises 10 control white-matter samples and rim and perilesional samples from 7 chronic active and 8 inactive lesions, supplied by the Netherlands Brain Bank; the number of distinct MS donors is not stated in the public record. GSE135511 (22) (Illumina HumanRef-8 v3, GPL6883) comprises motor-cortex samples from 10 controls and 20 MS donors; the groups used here were follicle-negative grey-matter lesions (GSM4013310–GSM4013319), follicle-positive grey-matter lesions (GSM4013320–GSM4013329) and follicle-negative normal-appearing grey matter (GSM4013330–GSM4013339), each against the same 10 controls (GSM4013300–GSM4013309). The follicle-negative lesion and normal-appearing samples come from the same 10 donors. The fifth group, follicle-positive normal-appearing grey matter (GSM4013340–GSM4013349), and the direct follicle-negative versus follicle-positive contrasts were analyzed from the series matrix with the limma implementation described below, with probes mapped through the GPL6883 annotation. GSE131279 (23) (Illumina HumanHT-12 V4.0, GPL10558) compares 37 cortical grey-matter lesion samples from 18 MS donors with 41 normal-appearing grey-matter samples from 20 MS donors; it is one of the two sub-series of GSE131282. GSE123496 (25) (Illumina HiSeq 3000, GPL21290) comprises 50 samples from five brain regions of five MS donors and five controls.

Per-cohort differential expression

Per-cohort MS-versus-control estimates for the meta-analysis were taken from NCBI GEO2R: DESeq2 results on NCBI-generated counts for GSE138614 (42) and limma results for GSE32915 and GSE108000 (43), with GSE138614 comprising the 72 MS samples present in the NCBI-generated counts (GSM4114316, a chronic active lesion sample, is absent from them) against the 25 controls, GSE32915 all 12 MS samples against the 4 controls, and GSE108000 all 30 MS samples against the 10 controls; the GSE32915 and GSE108000 tables were reproduced exactly from their series matrices, which confirms these groupings. No covariates were included, and samples from the same donor or lesion were treated as independent in every contrast. GSE108000 probes were mapped to gene symbols through the GPL13497 platform annotation because the GEO2R export lacked symbols. The lesion-zone (GSE108000), grey-matter (GSE135511, GSE131279) and GSE123496 contrasts also used GEO2R; complete result tables were exported and checked for completeness before use. GSE138614 lesion types were analyzed from the deposited count matrix with PyDESeq2 0.5.4 (44) (design ~ condition, each lesion type against the 25 control white-matter samples, default settings), and Ensembl gene identifiers were mapped to symbols with an Ensembl BioMart gene table. For comparison, the originating authors' deposited edgeR results for the same five contrasts, which account for repeated samples from the same patient and are adjusted for age and sex, agree in direction for every gene discussed in the text that they report. In all tiers, gene-level values used the probe or gene entry with the smallest P value; a panel hit in a single contrast was defined as Benjamini–Hochberg adjusted $P < 0.05$ and $|\log_2 \text{fold-change}| \geq 0.5$, and this effect-size floor applies to single-contrast counts only, not to the meta-analysis.

Random-effects meta-analysis

Per-gene effects were pooled on the log2 fold-change scale by inverse-variance random-effects meta-analysis with the DerSimonian–Laird estimator (45). Standard errors were lfcSE for the RNA-seq cohort and |logFC/t| for the microarray cohorts. Genes measured in at least two cohorts were meta-analyzable; P values were two-sided normal-approximation values, and multiple testing was controlled by Benjamini–Hochberg FDR across the 442 meta-analyzable panel genes (46). Nominal significance within a cohort, used by the high-confidence rule, was the two-sided normal-approximation P of that cohort's estimate divided by its standard error; the high-confidence set is identical when the GEO2R per-cohort P values are used instead. The locked high-confidence rule is FDR < 0.05, measured in ≥ 3 cohorts, direction-concordant in ≥ 70% of contributing cohorts, and nominally significant in ≥ 2 cohorts; with three cohorts, the direction criterion requires all three to agree in sign. For genes with several array probes, the probe with the smallest P value was used; because this choice depends on the outcome, a mean-probe analysis is reported as a sensitivity analysis. Heterogeneity is reported as I^2. With few studies, the DerSimonian–Laird estimator can underestimate between-study variance and give confidence intervals that are too narrow (47); a Hartung–Knapp–Sidik–Jonkman analysis is reported as a sensitivity analysis (below). The locked per-gene results were reproduced from the three cohort tables, and the reproduction, with full-precision P values and standard errors, is provided as Data S1. For OPLAH, GAMT and PPARG, the locked file records P = 0 because the pipeline's floating-point calculation underflowed; their full-precision values are given in Table 1 and Data S1.

Sensitivity analyses

Further sensitivity analyses, beyond the probe-collapse and panel-freeze analyses (Table S4), were added after the locked analysis, using the pipeline above. (i) Transcriptome background: the pipeline was applied unchanged to every gene measured in at least two cohorts (19,365 genes), with Benjamini–Hochberg FDR across all of them; panel and other genes were compared for FDR significance and for the high-confidence rule by Fisher's exact test, and the panel's count was compared with 20,000 random sets of 442 measured genes. Each cohort's median log2 fold-change, percentage of negative log2 fold-changes and percentage of genes at nominal P < 0.05 were computed from the same tables. (ii) Repeated samples: each cohort was re-fitted with the donor or lesion as the unit. For GSE138614, the NCBI-generated counts were summed per donor using the donor labels in the GEO sample annotations (10 MS and 5 control donors) and analyzed with PyDESeq2 0.5.4 (44) using the GEO2R settings (poscounts size factors; genes with at least 10 counts in at least 5 units); with these settings the sample-level GEO2R table is reproduced (log2 fold-change correlation > 0.9999). For GSE32915, log2 values were averaged per patient (4 versus 4); for GSE108000, rim and perilesional values were averaged per lesion (15 versus 10), because donor labels are not public. Array contrasts used a Python implementation of the limma model with empirical Bayes moderation (43), which reproduces both GEO2R tables exactly. As an approximation for comparison, each locked table's standard errors were also multiplied by the square root of $[(1 + (m1^* - 1)\rho)/n1 + (1 + (m2^* - 1)\rho)/n2] / (1/n1 + 1/n2)$, the design effect for clusters with size-weighted mean size $m^* = \Sigma m^2/n$ and within-cluster correlation ρ =

0.25, 0.5, 0.75 or 1 (GSE138614, n = 72 and 25, m* = 7.89 and 5; GSE32915, n = 12 and 4, m* = 3.17 and 1; GSE108000, n = 30 and 10, m* = 2 and 1). Composition: the donor-level models were re-fitted with an oligodendrocyte marker score (mean standardized expression of PLP1, MOG, MOBP, MBP, MAG and OPALIN), and then with a macrophage score (CD68, CD163 and CSF1R) added, as covariates. (iii) Hartung–Knapp–Sidik–Jonkman: the DerSimonian–Laird pooled estimate was tested with the Hartung–Knapp variance and a t distribution with k − 1 degrees of freedom (47). (iv) Marker transcripts in the bulk cohorts: log2 fold-changes of cell-type marker transcripts (oligodendrocyte, microglia and macrophage, astrocyte, endothelial) were read from the same tables. Analyses (i), (iii) and (iv) used only the per-cohort GEO2R tables; results are in Tables S4–S6 and Data S1.

Independent-cohort check of the high-confidence set

For each of the 30 high-confidence genes, the GSE123496 MS-versus-control log2 fold-change (GEO2R DESeq2 on NCBI-generated counts; complete table of 22,045 genes) was compared in sign with the pooled estimate. Direction concordance was tested against 50% by a two-sided exact binomial test, and Pearson and Spearman correlations with the pooled estimates were computed. The permutation baseline is the distribution of |r| over 5,000 random reassignments of GSE123496 estimates across all measurable panel genes. GSE123496 is the same external cohort used for MS in the methods-and-panel manuscript (1).

Exclusions

GSE38010 (GPL570; 5 MS lesions, 2 controls) was excluded because its series-matrix values are MAS5-scaled intensities on a linear scale (median about 300–390 per array, maximum above 37,000), not log-transformed values; GSE52139 (GPL570) compares spinal-cord periplaque with normal-appearing white matter within MS and has no non-MS control. GSE5839 (GPL96; three MS and one non-neurological control brain sample) was excluded because a single control array gives no replicate control group, so between-group differences cannot be separated from variation between individuals. GSE131282 (GPL10558; 142 MS versus 42 control grey-matter samples) was excluded for a transcriptome-wide scale offset, which arises from separate normalization of its two sub-series; its donor-level pseudoreplication is a further caveat (Results; Fig. 3). Its differential expression was computed from the series matrices of its sub-series (GSE131279 and GSE131281; limma, 142 MS versus 42 control samples). The original analysis mapped probes through the GPL6883 (Illumina HumanRef-8 v3) annotation, giving 18,630 genes, 427 panel genes and a median log2 fold-change of − 0.47; the analysis reported here maps them through the annotation of the array's own platform, GPL10558 (HumanHT-12 V4.0 manifest, release R1), giving 31,334 genes and 452 panel genes, and the offset is present under both mappings. The pooled series contributes to no pooled or reported estimate; its sub-series GSE131281 is reported alone as a supporting grey-matter contrast (normal-appearing grey matter against control; Results, Table 5, Fig. 3C), and also averaged per donor. GSE100297 (optic chiasm; 5 MS donors versus 5 controls; GPL21290) was screened and analyzed on the panel from its deposited gene counts (PyDESeq2, MS versus control): 32 of 391 tested panel genes reached FDR < 0.05, including higher HMOX1 (+ 2.20) and SLC40A1 (+ 0.80) and lower CLDN11. Of the 30 high-confidence genes, 29

were measured and 19 changed in the same direction (two-sided binomial p = 0.14; Pearson r = 0.69). Because optic chiasm is not brain white matter, and because the series comes from the same group and brain bank as GSE123496 and may share donors with it, GSE100297 is not used further; per-gene values are in Data S3.

Single-nucleus composition

Cell-level metadata for 632,375 nuclei from the single-nucleus atlas of Macnair et al. (24) (Zenodo, https://doi.org/10.5281/zenodo.8338963; file ms_lesions_snRNAseq_col_data_2023-09-12.txt) were used to compute broad cell-type fractions per lesion type for the 335,694 white-matter nuclei. No expression data from the atlas were analyzed.

Data and code

The locked panel, excluded-symbol list, pipeline and locked per-disease meta-analysis results are deposited at Zenodo (8). The per-gene meta-analysis reproduction (Data S1), the GSE138614 lesion-type re-analysis (Data S2), the lesion-zone and grey-matter contrasts (Data S3) and the grey-matter re-analyses behind Fig. 3 and the added GSE135511 contrasts (Data S4) accompany this paper as supplementary files.

Ethics and human subjects

The archived transcriptomic analyses used only publicly available, de-identified gene-expression data from the NCBI Gene Expression Omnibus and a public single-nucleus metadata file; those datasets carry the ethical oversight of their originating studies. No identifiable private information was accessed, and no living human subjects were enrolled, recruited, or intervened upon by the author.

Declarations

Companion note. This paper is a disease-restricted multiple sclerosis analysis that uses the locked 468-gene panel and high-confidence rule of the methods-and-panel manuscript of this series (1). It is not a pooled cross-disease analysis. Four parallel companion manuscripts apply the same panel and rule to one disease each; the methods-and-panel manuscript holds the panel definition and the list-level permutation analysis, which are not repeated here. The methods-and-panel manuscript reports the MS white-matter counts as part of its cross-disease synthesis; this paper reports the full MS analysis, its independent-cohort check and the supporting lesion, grey-matter and composition tiers.

One-sentence summary. Three white-matter cohorts yield 30 high-confidence panel-gene associations, 25 of which change in the same direction in an independent cohort; re-fitted with the donor as the unit, 12 of the 30 remain high-confidence, and panel genes change little more often than other genes; higher HMOX1 and lower GPX4 transcript abundance recur in supporting lesion tiers, and neither demonstrates ferroptosis.

Ethics and human subjects

The archived transcriptomic analyses used only publicly available, de-identified gene-expression data from the NCBI Gene Expression Omnibus and a public single-nucleus metadata file; those datasets carry the ethical oversight of their originating studies. No identifiable private information was accessed, and no living human subjects were enrolled, recruited, or intervened upon by the author.

Consent for publication

Not applicable.

Declaration of generative AI

During the preparation of this work the author used Grok (xAI), Claude (Anthropic), and Perplexity to assist with literature synthesis, bioinformatic pipeline construction, editorial refinement, and critical review of claims and citations. After using these tools, the author reviewed and edited the content and takes full responsibility for the content of the article. No generative tool is an author.

Acknowledgments

The author thanks the investigators who generated and deposited the datasets analyzed in this work, and acknowledges the participants in the original studies.

Funding

This multiple sclerosis analysis received no external funding and was conducted independently through Sirius Neuroscience, LLC. Sequencing and liver-tissue purchase that supported the author's prior Alzheimer disease study (6) were funded by Daniel Foley; that support did not fund the present analysis.

Author contributions

M.E.M. is the sole author and performed all aspects of this work: conceptualization, panel application, dataset analysis, interpretation, and manuscript writing.

Competing interests

The author is the sole inventor on a filed patent application relating to panel-based research scoring methods that use the locked 468-gene list reported here. The application did not determine gene

membership, the high-confidence rule, or the reported results. Academic reuse of the deposited panel and code does not require a license from the author. The author declares no other competing interests.

Data and materials availability

All cohorts are public GEO accessions listed in Materials and Methods. The locked 468-gene panel, excluded-symbol list, analysis pipeline and locked per-disease meta-analysis results, including the MS per-gene table (version 1.1), are deposited at Zenodo (8). Tables S1–S6 and Data S1–S4 accompany this paper. Figures 1–3 are provided as separate high-resolution files.

References

1. M. E. McCaulley, Transcriptomic associations of a pre-specified 468-gene redox and xenobiotic-metabolism panel across five neurological disorders, with a published-variant inventory. Methods-and-panel manuscript of this series, under peer review at Molecular Neurobiology (2026).
2. C. Walton, R. King, L. Rechtman, W. Kaye, E. Leray, R. A. Marrie, N. Robertson, N. La Rocca, B. Uitdehaag, I. van der Mei et al., Rising prevalence of multiple sclerosis worldwide: insights from the Atlas of MS, third edition. Mult. Scler. 26, 1816–1821 (2020). https://doi.org/10.1177/1352458520970841
3. M. Filippi, A. Bar-Or, F. Piehl, P. Preziosa, A. Solari, S. Vukusic, M. A. Rocca, Multiple sclerosis. Nat. Rev. Dis. Primers 4, 43 (2018). https://doi.org/10.1038/s41572-018-0041-4
4. H. Lassmann, J. van Horssen, D. Mahad, Progressive multiple sclerosis: pathology and pathogenesis. Nat. Rev. Neurol. 8, 647–656 (2012). https://doi.org/10.1038/nrneurol.2012.168
5. D. H. Mahad, B. D. Trapp, H. Lassmann, Pathological mechanisms in progressive multiple sclerosis. Lancet Neurol. 14, 183–193 (2015). https://doi.org/10.1016/S1474-4422(14)70256-X
6. M. E. McCaulley, Impaired pathways of detoxification and risk of Alzheimer's disease: differential gene expression studies via gene set expression analysis. J. Alzheimers Dis. Rep. 10, 25424823261419382 (2026). https://doi.org/10.1177/25424823261419382
7. J. X. Santos, C. Rasga, A. R. Marques, H. Martiniano, M. Asif, J. Vilela, G. Oliveira, L. Sousa, A. Nunes, A. M. Vicente, A role for gene-environment interactions in autism spectrum disorder is supported by variants in genes regulating the effects of exposure to xenobiotics. Front. Neurosci. 16, 862315 (2022). https://doi.org/10.3389/fnins.2022.862315
8. M. E. McCaulley, Locked 468-gene detoxification panel, excluded-symbol list, analysis pipeline and per-disease meta-analysis results. Zenodo, version 1.0 (2026), https://doi.org/10.5281/zenodo.22178094; version 1.1 (2026), https://doi.org/10.5281/zenodo.22181129; all versions, https://doi.org/10.5281/zenodo.22178093.
9. R. Gold, L. Kappos, D. L. Arnold, A. Bar-Or, G. Giovannoni, K. Selmaj, C. Tornatore, M. T. Sweetser, M. Yang, S. I. Sheikh, K. T. Dawson; DEFINE Study Investigators, Placebo-controlled phase 3 study of

oral BG-12 for relapsing multiple sclerosis. N. Engl. J. Med. 367, 1098–1107 (2012). https://doi.org/10.1056/NEJMoa1114287. Erratum: N. Engl. J. Med. 367, 2362 (2012).

10. R. J. Fox, D. H. Miller, J. T. Phillips, M. Hutchinson, E. Havrdova, M. Kita, M. Yang, K. Raghupathi, M. Novas, M. T. Sweetser et al., Placebo-controlled phase 3 study of oral BG-12 or glatiramer in multiple sclerosis. N. Engl. J. Med. 367, 1087–1097 (2012). https://doi.org/10.1056/NEJMoa1206328
11. E. Van San, A. C. Debruyne, G. Veeckmans, Y. Y. Tyurina, V. A. Tyurin, H. Zheng, S. M. Choi, K. Augustyns, G. van Loo, B. Michalke et al., Ferroptosis contributes to multiple sclerosis and its pharmacological targeting suppresses experimental disease progression. Cell Death Differ. 30, 2092–2103 (2023). https://doi.org/10.1038/s41418-023-01195-0
12. P. Jhelum, S. Zandee, F. Ryan, J. G. Zarruk, B. Michalke, V. Venkataramani, L. Curran, W. Klement, A. Prat, S. David, Ferroptosis induces detrimental effects in chronic EAE and its implications for progressive MS. Acta Neuropathol. Commun. 11, 121 (2023). https://doi.org/10.1186/s40478-023-01617-7
13. T. Wu, S. Ning, H. Zhang, Y. Cao, X. Li, J. Hao, L. Wang, Role of ferroptosis in neuroimmunity and neurodegeneration in multiple sclerosis revealed by multi-omics data. J. Cell. Mol. Med. 28, e18396 (2024). https://doi.org/10.1111/jcmm.18396
14. L. Stojkovic, A. Djordjevic, M. Stefanovic, A. Stankovic, E. Dincic, T. Djuric, M. Zivkovic, Circulatory indicators of lipid peroxidation, the driver of ferroptosis, reflect differences between relapsing–remitting and progressive multiple sclerosis. Int. J. Mol. Sci. 25, 11024 (2024). https://doi.org/10.3390/ijms252011024
15. S.-C. Gu, C.-X. Yuan, C. Gu, Identification of ferroptosis-related gene signatures associated with multiple sclerosis using weighted gene co-expression network analysis. Medicine (Baltimore) 101, e31802 (2022). https://doi.org/10.1097/MD.0000000000031802
16. X. Wang, T. Chen, S. Chen, J. Zhang, L. Cai, C. Liu, Y. Zhang, X. Wu, N. Li, Z. Ma et al., STING aggravates ferroptosis-dependent myocardial ischemia-reperfusion injury by targeting GPX4 for autophagic degradation. Signal Transduct. Target. Ther. 10, 136 (2025). https://doi.org/10.1038/s41392-025-02216-9
17. M. S. Woo, C. Mayer, L. Binkle-Ladisch, J. K. Sonner, S. C. Rosenkranz, A. Shaposhnykov, N. Rothammer, V. Tsvilovskyy, S. M. Lorenz, L. Raich et al., STING orchestrates the neuronal inflammatory stress response in multiple sclerosis. Cell 187, 4043–4060.e30 (2024). https://doi.org/10.1016/j.cell.2024.05.031
18. W. Wang, M. Guo, X. Tu, M. Jiang, C.-J. Zhang, Neuronal STING activation mediates inflammation-induced neurodegeneration via ferroptosis pathways in multiple sclerosis. Biophys. Rep. 10, 416 (2024). https://doi.org/10.52601/bpr.2024.240908
19. M. L. Elkjaer, T. Frisch, R. Reynolds, T. Kacprowski, M. Burton, T. A. Kruse, M. Thomassen, J. Baumbach, Z. Illes, Molecular signature of different lesion types in the brain white matter of patients with progressive multiple sclerosis. Acta Neuropathol. Commun. 7, 205 (2019). https://doi.org/10.1186/s40478-019-0855-7

20. M. T. Fischer, R. Sharma, J. L. Lim, L. Haider, J. M. Frischer, J. Drexhage, D. Mahad, M. Bradl, J. van Horssen, H. Lassmann, NADPH oxidase expression in active multiple sclerosis lesions in relation to oxidative tissue damage and mitochondrial injury. Brain 135, 886–899 (2012). https://doi.org/10.1093/brain/aws012
21. D. A. E. Hendrickx, J. van Scheppingen, M. van der Poel, K. Bossers, K. G. Schuurman, C. G. van Eden, E. M. Hol, J. Hamann, I. Huitinga, Gene expression profiling of multiple sclerosis pathology identifies early patterns of demyelination surrounding chronic active lesions. Front. Immunol. 8, 1810 (2017). https://doi.org/10.3389/fimmu.2017.01810
22. R. Magliozzi, O. W. Howell, P. Durrenberger, E. Aricò, R. James, C. Cruciani, C. Reeves, F. Roncaroli, R. Nicholas, R. Reynolds, Meningeal inflammation changes the balance of TNF signalling in cortical grey matter in multiple sclerosis. J. Neuroinflammation 16, 259 (2019). https://doi.org/10.1186/s12974-019-1650-x
23. L. S. Enz, T. Zeis, D. Schmid, F. Geier, F. van der Meer, G. Steiner, U. Certa, T. M. C. Binder, C. Stadelmann, R. Martin, N. Schaeren-Wiemers, Increased HLA-DR expression and cortical demyelination in MS links with HLA-DR15. Neurol. Neuroimmunol. Neuroinflamm. 7, e656 (2020). https://doi.org/10.1212/NXI.0000000000000656
24. W. Macnair, D. Calini, E. Agirre, J. Bryois, S. Jäkel, R. S. Smith, P. Kukanja, N. Stokar-Regenscheit, V. Ott, L. C. Foo et al., snRNA-seq stratifies multiple sclerosis patients into distinct white matter glial responses. Neuron 113, 396–410.e9 (2025). https://doi.org/10.1016/j.neuron.2024.11.016
25. R. R. Voskuhl, N. Itoh, A. Tassoni, M. A. Matsukawa, E. Ren, V. Tse, E. Jang, T. T. Suen, Y. Itoh, Gene expression in oligodendrocytes during remyelination reveals cholesterol homeostasis as a therapeutic target in multiple sclerosis. Proc. Natl. Acad. Sci. U.S.A. 116, 10130–10139 (2019). https://doi.org/10.1073/pnas.1821306116
26. S. Hametner, I. Wimmer, L. Haider, S. Pfeifenbring, W. Brück, H. Lassmann, Iron and neurodegeneration in the multiple sclerosis brain. Ann. Neurol. 74, 848–861 (2013). https://doi.org/10.1002/ana.23974
27. M. Absinta, P. Sati, F. Masuzzo, G. Nair, V. Sethi, H. Kolb, J. Ohayon, T. Wu, I. C. M. Cortese, D. S. Reich, Association of chronic active multiple sclerosis lesions with disability in vivo. JAMA Neurol. 76, 1474–1483 (2019). https://doi.org/10.1001/jamaneurol.2019.2399
28. M. Absinta, P. Sati, M. Schindler, E. C. Leibovitch, J. Ohayon, T. Wu, A. Meani, M. Filippi, S. Jacobson, I. C. M. Cortese, D. S. Reich, Persistent 7-tesla phase rim predicts poor outcome in new multiple sclerosis patient lesions. J. Clin. Invest. 126, 2597–2609 (2016). https://doi.org/10.1172/JCI86198
29. A. A. Chora, P. Fontoura, A. Cunha, T. F. Pais, S. Cardoso, P. P. Ho, L. Y. Lee, R. A. Sobel, L. Steinman, M. P. Soares, Heme oxygenase-1 and carbon monoxide suppress autoimmune neuroinflammation. J. Clin. Invest. 117, 438–447 (2007). https://doi.org/10.1172/JCI28844
30. H. M. Schipper, W. Song, A. Tavitian, M. Cressatti, The sinister face of heme oxygenase-1 in brain aging and disease. Prog. Neurobiol. 172, 40–70 (2019). https://doi.org/10.1016/j.pneurobio.2018.06.008

31. Y. Ma, D. Zhang, Z. Li, Dual role of heme oxygenase-1 in disease progression and treatment: a literature review. Int. J. Biol. Macromol. 321, 146272 (2025). https://doi.org/10.1016/j.ijbiomac.2025.146272
32. A. S. Ferecskó, M. J. Smallwood, A. Moore, C. Liddle, J. Newcombe, J. Holley, J. Whatmore, N. J. Gutowski, P. Eggleton, STING-triggered CNS inflammation in human neurodegenerative diseases. Biomedicines 11, 1375 (2023). https://doi.org/10.3390/biomedicines11051375
33. Y. Yang, F. Cai, N. Zhou, S. Liu, P. Wang, S. Zhang, Y. Zhang, A. Zhang, Z. Jia, S. Huang, Dimethyl fumarate prevents ferroptosis to attenuate acute kidney injury by acting on NRF2. Clin. Transl. Med. 11, e382 (2021). https://doi.org/10.1002/ctm2.382
34. A. P. Gunn, J. B. W. Hilton, S. Mukherjee, J. R. Liddell, S. W. Mercer, C. A. McLean, C. L. Masters, P. J. Crouch, B. R. Roberts, Decreased metallothionein-3 expression in the human spinal cord is a common feature of amyotrophic lateral sclerosis and multiple sclerosis. Sci. Rep. 16, 9598 (2026). https://doi.org/10.1038/s41598-025-31283-9
35. M. E. McCaulley, A locked 468-gene detoxification panel in Alzheimer's disease brain, liver, and blood: 141 high-confidence cerebral associations including lower CYP46A1 transcript abundance, and a 12-sample hepatic CYP7A1 signal. Research Square, version 1 (2026). https://doi.org/10.21203/rs.3.rs-10999456/v1
36. M. E. McCaulley, Panel-gene transcriptomic associations and published-variant architecture in Parkinson disease. Research Square, version 1 (2026). https://doi.org/10.21203/rs.3.rs-11097203/v1
37. M. E. McCaulley, Panel-gene transcriptomic associations in amyotrophic lateral sclerosis: a donor-resolved seven-cohort analysis of a locked 468-gene detoxification panel. Companion manuscript of this series, in preparation (2026).
38. M. E. McCaulley, A null adult postmortem-brain test of a locked 468-gene panel in autism spectrum disorder, with published maternal-axis architecture as context. Companion manuscript of this series, in preparation (2026).
39. R. Magliozzi, O. W. Howell, C. Reeves, F. Roncaroli, R. Nicholas, B. Serafini, F. Aloisi, R. Reynolds, A gradient of neuronal loss and meningeal inflammation in multiple sclerosis. Ann. Neurol. 68, 477–493 (2010). https://doi.org/10.1002/ana.22230
40. H. Lassmann, J. van Horssen, Oxidative stress and its impact on neurons and glia in multiple sclerosis lesions. Biochim. Biophys. Acta Mol. Basis Dis. 1862, 506–510 (2016). https://doi.org/10.1016/j.bbadis.2015.09.018
41. S. Licht-Mayer, I. Wimmer, S. Traffehn, I. Metz, W. Brück, J. Bauer, M. Bradl, H. Lassmann, Cell type-specific Nrf2 expression in multiple sclerosis lesions. Acta Neuropathol. 130, 263–277 (2015). https://doi.org/10.1007/s00401-015-1452-x
42. M. I. Love, W. Huber, S. Anders, Moderated estimation of fold change and dispersion for RNA-seq data with DESeq2. Genome Biol. 15, 550 (2014). https://doi.org/10.1186/s13059-014-0550-8

43. M. E. Ritchie, B. Phipson, D. Wu, Y. Hu, C. W. Law, W. Shi, G. K. Smyth, limma powers differential expression analyses for RNA-sequencing and microarray studies. Nucleic Acids Res. 43, e47 (2015). https://doi.org/10.1093/nar/gkv007
44. B. Muzellec, M. Teleńczuk, V. Cabeli, M. Andreux, PyDESeq2: a python package for bulk RNA-seq differential expression analysis. Bioinformatics 39, btad547 (2023). https://doi.org/10.1093/bioinformatics/btad547
45. R. DerSimonian, N. Laird, Meta-analysis in clinical trials. Control. Clin. Trials 7, 177–188 (1986). https://doi.org/10.1016/0197-2456(86)90046-2
46. Y. Benjamini, Y. Hochberg, Controlling the false discovery rate: a practical and powerful approach to multiple testing. J. R. Stat. Soc. B 57, 289–300 (1995). https://doi.org/10.1111/j.2517-6161.1995.tb02031.x
47. J. IntHout, J. P. A. Ioannidis, G. F. Borm, The Hartung-Knapp-Sidik-Jonkman method for random effects meta-analysis is straightforward and considerably outperforms the standard DerSimonian-Laird method. BMC Med. Res. Methodol. 14, 25 (2014). https://doi.org/10.1186/1471-2288-14-25

Figures

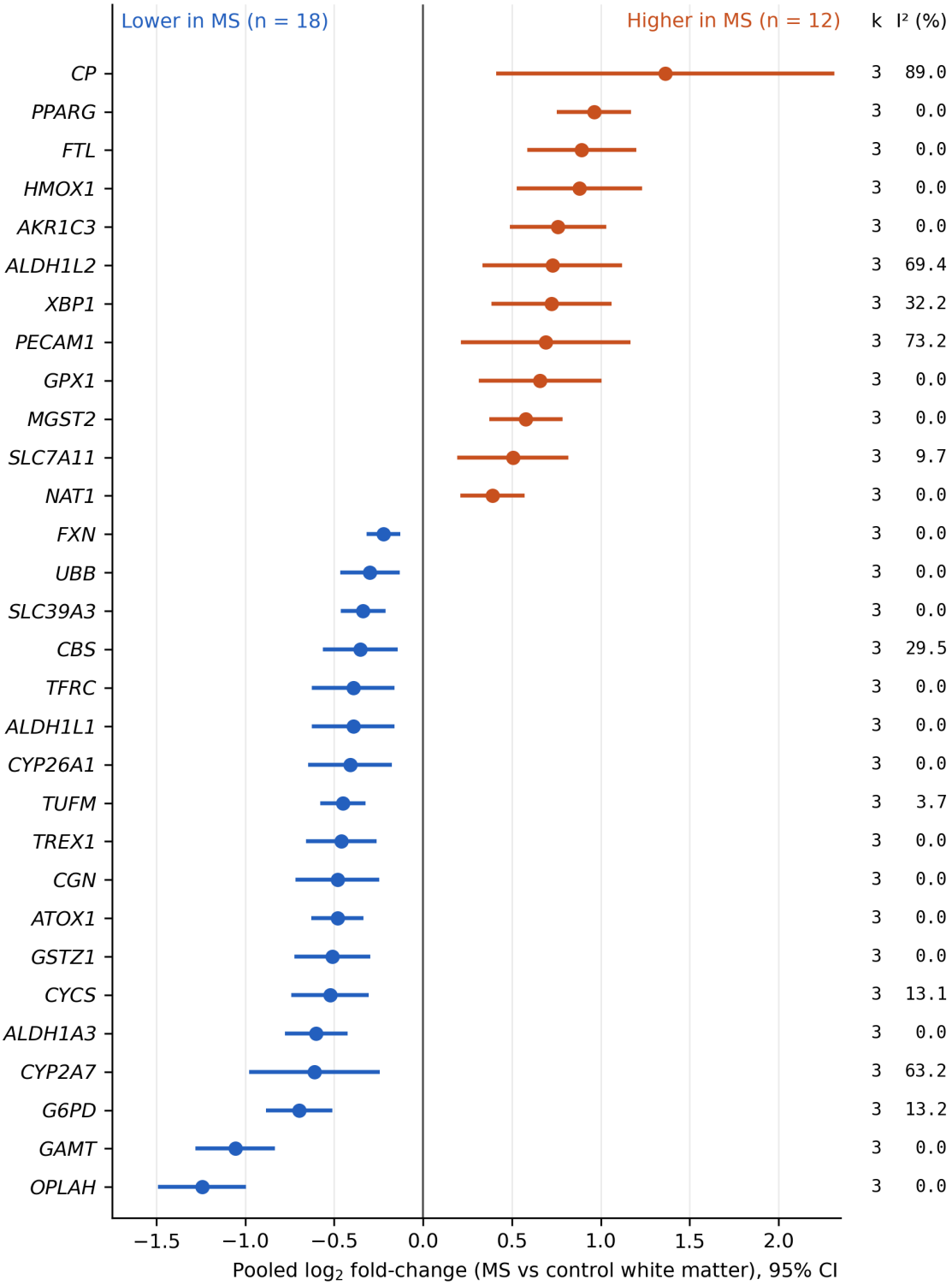


Figure 1

The 30 high-confidence genes of the three-cohort white-matter meta-analysis. Points are pooled log2 fold-changes (MS vs control white matter; DerSimonian–Laird random effects across GSE138614, GSE32915 and GSE108000) and bars are 95% confidence intervals (pooled estimate ± 1.96 × SE). Orange, higher in MS (n = 12); blue, lower in MS (n = 18). k (number of contributing cohorts) and I² are printed at the right of each row. High-confidence rule: FDR < 0.05, measured in ≥ 3 cohorts, direction-

concordant in ≥ 70% of contributing cohorts, nominally significant in ≥ 2 cohorts. Standard errors are from the reproduction of the locked analysis (Data S1).

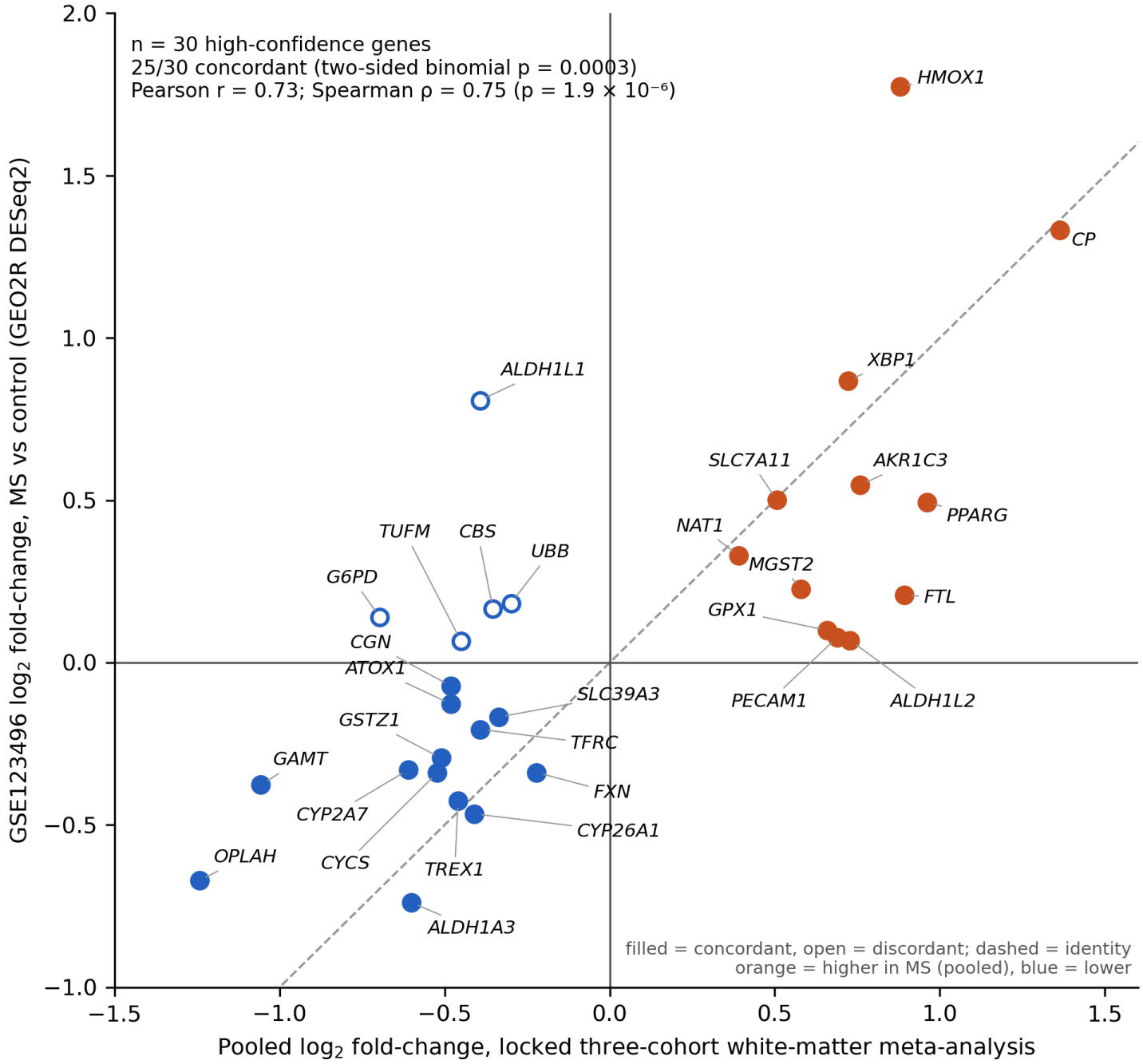


Figure 2

Independent-cohort check of the 30 high-confidence genes in GSE123496. Each point is one gene: pooled log2 fold-change from the three locked white-matter cohorts (horizontal) against the GSE123496 MS-versus-control log2 fold-change (vertical; NCBI GEO2R DESeq2 on NCBI-generated counts; five brain regions from five MS donors and five controls). Orange, higher in MS in the pooled analysis; blue, lower. Filled symbols are direction-concordant and open symbols discordant; the dashed line is identity.

Twenty-five of 30 genes are concordant (two-sided exact binomial p = 0.0003); Pearson r = 0.73; Spearman ρ = 0.75 ($p = 1.9 \times 10^{-6}$). Per-gene values are in Table S3.

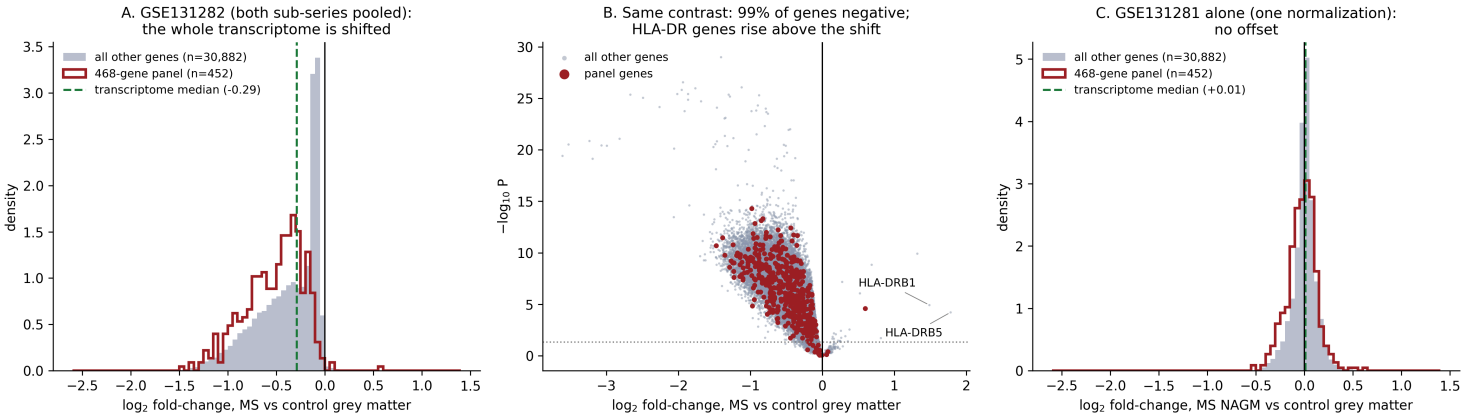


Figure 3

Exclusion of GSE131282. A: distribution of MS-versus-control log2 fold-changes in cortical grey matter in the pooled series for the 452 measurable panel genes (red outline) and the other 30,882 genes (grey fill), each shown as a density; the dashed line marks the transcriptome-wide median of −0.29. B: the same contrast as a volcano plot, with panel genes in red; the dotted line marks FDR = 0.05. Ninety-nine per cent of measured genes are negative, and the genes rising clearly above the offset include HLA-DRB1 and HLA-DRB5, the finding reported by the originating study. C: the same distributions for GSE131281 alone (64 MS normal-appearing grey-matter samples against 42 control samples, one normalization), where no offset is present (median +0.01). Values are limma estimates from the GSE131279 and GSE131281 series matrices (184 samples, Illumina GPL10558; probes mapped with the GPL10558 annotation; Data S4).

Supplementary Files

This is a list of supplementary files associated with this preprint. Click to download.

- McCaulleyMSDataS4greymatterreanalyses20261014.xlsx
- McCaulleyMSDataS3lesionzoneandgreymattercontrasts20261014.xlsx
- McCaulleyMSDataS2GSE138614lesiontypes20261014.xlsx
- McCaulleyMSDataS1metapergene20260930.xlsx
- McCaulleyMS468panelSupplementaryMaterials20261014.docx